UNIVERSIDAD DE COSTA RICA
SISTEMA DE ESTUDIOS DE POSGRADO

DESARROLLO Y ANÁLISIS DEL COMPORTAMIENTO HUMANO ADAPTIVO EN MODELOS CON RELAPSO NO LINEAL

Development and analysis of human adaptive behavior in a model with non-linear relapse

Trabajo final de investigación aplicada sometido a la consideración de la Comisión del Programa de Posgrado en Matemática para optar al grado y título de Maestría Profesional en Métodos Matemáticos y Aplicaciones.

JIMMY JOSÉ CALVO MONGE

Ciudad Universitaria Rodrigo Facio, Costa Rica
2023

Dedicatoria

A mi madre, doña Rosa.

Agradecimientos

En primer lugar quiero expresar un enorme agradecimiento a mi asesor de tesis, el Dr. Fabio Sánchez. Desde años antes de iniciar con este proyecto he contado con su apoyo y confianza incondicionales, y al emprender este proyecto me ha demostrado que continúa dispuesto a ofrecerme toda la ayuda posible. He aprendido mucho de él -tanto académica como interpersonalmente- y me siento orgulloso de formar parte de sus esfuerzos de investigación y de poder contar con su sabio consejo y apoyo. ¡Gracias Fabio por creer en mí y siempre pensar en mi futuro y cómo prepararme lo mejor posible para afrontar las oportunidades que vienen de camino! Me gustaría también agradecer a mis asesores, Juan Gabriel Calvo y Darío Mena, quienes me han apoyado muy amablemente durante este trabajo. Ustedes han creído de verdad en este esfuerzo de investigación desde sus inicios y me han dado valiosos consejos durante este camino tan enriquecedor. En resumen, a mi equipo asesor les agradezco infinitamente por permitirme cumplir mi meta de obtener un título de posgrado en matemática aplicada, pero de manera mucho más importante, les agradezco por colaborar conmigo en la producción y publicación de nuevos resultados en investigación. Con esto me han brindado la experiencia y enorme gratificación de contribuir al desarrollo en investigación en matemática aplicada. ese es el producto más valioso que me llevo de este proyecto con ustedes. Culminando el proyecto de esta maestría profesional agradezco también a todos los profesores que con gran esfuerzo y profesionalismo me impartieron conocimientos que serán sin duda invaluables para mi desarrollo profesional, como Análisis de Datos, Estadística, Probabilidad Avanzada, Álgebra Lineal Numérica, Series de Tiempo y Programación Matemática; fue una muy buena experiencia académica para mí. Finalmente agradezco a mi familia, mi madre y mis hermanos, a mis amigos más cercanos, quienes siempre han creído en mí y me han hecho saber su orgullo por mi trabajo y mis proyectos de vida.

Este trabajo final de investigación aplicada fue aceptado por la Comisión del Programa de Posgrado en Matemática de la Universidad de Costa Rica, como requisito parcial para optar al grado y título de Maestría Profesional en Métodos Matemáticos y Aplicaciones.

Dr. Javier Trejos Zelaya
Representante del Decano del Sistema de Estudios de Posgrado

Dr. Fabio Sánchez Peña
Profesor Guía

Dr. Juan Gabriel Calvo Alpízar
Lector

Dr. Dario Mena Arias
Lector

Dr. Luis Barboza Chinchilla
Representante del Programa de Posgrado en Matemática

Jimmy José Calvo Monge
Sustentante

Contents

Resumen

En este proyecto proponemos estudiar las propiedades teóricas y nuevas aplicaciones de un algoritmo de formulación recuente para modelar las decisiones de contacto humanas en modelos epidemiológicos, que es llamado el algoritmo adaptativo o la metodología adaptativa. Esta metodología se propuso por primera vez en el artículo seminal [15] como resultado de un grupo de estudio cuyo objetivo era construir un enfoque de modelización en el que el proceso de toma de decisiones diarias individuales pudiera tenerse en cuenta en el proceso de simulación de una enfermedad. Desde entonces, el algoritmo adaptativo se ha utilizado para crear simulaciones de epidemias más realistas y se ha aplicado en varios contextos [13, 12, 26, 40, 2, 14]. La idea general que subyace a los algoritmos adaptativos es que los individuos realizan cada día un proceso de decisión sobre el número de contactos con los que deben relacionarse, y este proceso depende de varios factores. Consideramos dos tipos de factores que pueden afectar a la decisión de contacto de un agente, en primer lugar está el factor epidemiológico, que incluye el estado de salud actual del individuo, y el estado actual de la enfermedad (número actual de infectados, susceptibles, recuperados). El otro factor principal a tener en cuenta es el económico. En realidad, los agentes tienen necesidades económicas apremiantes para entablar contactos con otras personas. El enfoque adaptativo propone que el agente tome una decisión sobre el número de contactos diarios, ponderando la prevalencia de la enfermedad y su estado de salud actual frente a la utilidad económica que aporta cada contacto. Implementamos la configuración adaptativa completa también con fenómenos de no recaída y observamos mediante simulaciones cómo el comportamiento de los individuos susceptibles y parcialmente recuperados debe adaptarse al progreso de la enfermedad. El trabajo se encuentra desarrollado en inglés.

Abstract

In this project we propose to study theoretical properties and new applications of a recent algorithm to model human contact decisions in epidemiological models, which is called the *adaptive algorithm* or adaptive setting. This methodology was first proposed in the seminal paper [15] as the result of a study group whose focus was to construct a modelling approach in which the process of individual daily decision making can be taken into account in the simulation process of a disease. Since then the adaptive algorithm has been used to create more realistic epidemic simulations and has been applied in several contexts [13, 12, 26, 40, 2, 14]. The general idea behind adaptive algorithms is that individuals perform a decision process each day, regarding how many contacts they should engage with, and this process depends on several factors. We consider two types of factors that can affect the contact decision of an agent, first there is the epidemiological factor, which includes the individual's current health status, and the current status of the disease (current number of infected, susceptible, recovered). The other main factor to consider is the economical one. In reality, agents have pressing economical needs to engage in contacts with others. The adaptive approach thus proposes that the agent performs a decision on how many contacts to engage with daily, by weighting the disease prevalence and their current health status versus the economical utility brought by each contact number. We implement the full adaptive setting also with non-relapse phenomena and we observe through simulations how the behaviour of both susceptible and partially recovered individuals needs to adapt to the disease progress.

S	Susceptible population
I	Infected population
R	Recovered population without possibility of reinfection
$\widetilde{S}$	Recovered population with possibility of reinfection
E	Exposed population
$g(\cdot)$	Incidence rate function
$J(s,i,r)$	Jacobian of a SIR system
C^h	Contact rate for individuals of health class $h \in \{S, E, I, R \text{ or } \widetilde{S}\}$
u^h	Utility function for individuals of health class $h \in \{S, E, I, R \text{ or } \widetilde{S}\}$
R_0	Basic reproduction number
$\text{Ind}_x(f)$	Cauchy index of a function f at a point x
$\text{Ind}_a^b(f)$	Cauchy index of a function f at an interval $[a,b]$
$\mathcal{M}$	Markov Decision Process (MDP)
$\mathcal{A}$	Space of actions
$\mathcal{S}$	Space of states
$p_{hh'}^t(a)$	Probability transition function from state h to state h' in time t
π	A policy in a MDP
π^*	An optimal policy in a MDP
$V_t(h)$	Value function for state h at time t for an optimal policy in a MDP
C_{opt}^{h*}	optimal of the utility function $u^h(a)$
$\Delta(C^h)$	Maximum difference between any contact decision made by agent in state h in a MDP and their optimal immediate reward contact decision
R_0^{apparent}	Apparent R_0 in an adaptive behaviour model
$\|\|1/(u^h)''\|\|_{\infty,I}$	Maximum of inverse of utility function u^h at interval I
p_i	Probability that node i of a network becomes infected

List of Figures

Introduction

In this project we propose to study theoretical properties and new applications of a recent algorithm to model human contact decisions in epidemiological models, which is called the *adaptive algorithm* or adaptive setting. This methodology was first proposed in the seminal paper [15] as the result of a study group whose focus was to construct a modelling approach in which the process of individual daily decision making can be taken into account in the simulation process of a disease. Since then the adaptive algorithm has been used to create more realistic epidemic simulations and has been applied in several contexts [13, 12, 26, 40, 2, 14].

The general idea behind adaptive algorithms is that individuals perform a decision process each day, regarding how many contacts they should engage with, and this process depends on several factors. We consider two types of factors that can affect the contact decision of an agent, first there is the epidemiological factor, which includes the individual's current health status, and the current status of the disease (current number of infected, susceptible, recovered). It is natural that healthy agents have a different contact policy than those that are infected, and the difference can also occur between recovered people and those that haven't acquired the disease yet.

The other main factor to consider is the economical one. In reality, agents have pressing economical needs to engage in contacts with others. A teaching of the recent COVID-19 pandemic is that economic considerations should not be left aside when modeling the outbreak of an epidemic, as one of the great impacts on society that a pandemic has, besides the health impact, is the economical one [29]. When incorporating economical considerations into individual decision making, the usual approach is to specify individual utility functions. The adaptive approach thus proposes that the agent performs a decision on how many contacts to engage with daily, by weighting the disease prevalence and their current health status versus the economical utility brought by each contact number. This comparison creates a framework that merges both factors and yields a final response or decision.

In summary, this new approach requires two steps: first, to divide behavior by health status and second, to compute decisions also based on individual economical utility. Both steps are explored in chapters one and two of this thesis respectively, as we prepare in subsection below. The decision individuals make on how many contacts to engage with is updated each day and it takes into account the current status of the disease. The specific implementation of this comparison and weighted decision process is done using a tool from reinforcement learning called a **Markov Decision Process** and it is a mathematical construction to arrive to an optimal decision that combines the restrictions from the disease and the individual economical utility. We will describe this tool and it's application to the adaptive algorithm in Chapter 2.

The adaptive setting allows for a more realistic modelling strategy of the disease agents behavior and it has several impacts on the final disease equilibrium and disease prevalence in comparison with the classical models, which in turn assume that the behavior of agents remains constant throughout the epidemic development (a sometimes unrealistic assumption that this new adaptive approach aims to break with). The only disadvantage of this new proposal is that it becomes increasingly difficult to study analytically. As we will see in Chapter 2, the fact that the proposed epidemiological

system keeps updating daily prevents a classical analysis using the initial conditions and parameters of the system. We will obtain some partial theoretical results and with some simulations we will attempt to show the many theoretical challenges of this new methodology.

Chapter 1 will allow us to solve the incorporation of the first factor aforementioned: the epidemiological status of individuals. Our technique consists in performing a disaggregation of contact behavior per health status, thus avoiding that the same contact decisions are made by individuals of different health conditions. We prove several analytic results which demonstrate that the system's long term behavior is highly dependant of the relations between contact rates for individuals of different health classes.

An important issue so far not extensively studied with the adaptive setting is the presence of non-linear relapse phenomena. To our knowledge, the applications of adaptive algorithms so far have used models with no relapse. Addition of relapse behavior often brings out more complex equilibria scenarios, such as backwards bifurcation for example [18]; so we believe that it consists of an important phenomenon to study, specially with the new adaptive approach. The health contact disaggregation performed in Chapter 1 uses non-linear relapse phenomena and as the reader will see, brings out interesting bifurcation cases. In Chapter 2 we implement the full adaptive setting also with non-relapse phenomena and we observe through simulations how the behaviour of both susceptible and partially recovered individuals needs to adapt to the disease progress.

We believe the adaptive approach comes to change greatly the formulation of classical epidemic models and it creates a path for performing more realistic model simulations that incorporate a true decision process at the individual level. As the reader will verify, there are several theoretical and experimental challenges to this new methodology. We invite the reader to study our numerical implementations and explore this new method in applications to real-world disease simulations. Our main goal with this project is to set up a strong theoretical basis to fully understand the adaptive setting and it's advantages and challenges.

Organization of this thesis. This project consists of two chapters. In chapter one we explore the effects of adding contact rates per health status in a model with non-linear relapse. In this analysis contact rates for each health class are kept constant (for analytical simplicity). We propose a new incidence function and present our model, then we obtain some theoretical results regarding the existence of equilibria points and stability. These results are proved using some algebraical tools, and in great part they generalize corresponding results obtained in a previous study of non-relapse phenomena ([32]). Next, we perform some numerical examples highlighting the impact that the ratios of the different contact rates have on the model asymptotic behavior and finally we make discussions of the real-world impact of this methodology on modeling relapse phenomena. The results of this chapter can be found in [7].

In chapter two we proceed to investigate the adaptive algorithm more in depth. To understand it we start by recounting the theory of Markov Decision Processes, in order to explain how it is applied in devising the adaptive algorithm, process that we present in detail. After the theory and implementation of the adaptive algorithm is finalized we present several numerical examples in models with and without relapse in order to show the impact that the adaptive setting has on

the model's performance and on the disease equilibrium and asymptotic behavior. In this section we also perform some experiments so see how the model's parameters affect the severity of the adaptive consideration process and we formulate some conjectures on this behavior, which are discussed heuristically and confirmed with some experiments (even in [15]). In the next section we prove some theoretical results on the numerical conjectures found in the experiments section. Finally, we finalize chapter two with an application of the adaptive setting to epidemiological network models. Based on the groundbreaking multi-layer network model proposed in [35], we use the theory of adaptive behavior to incorporate a contact decision making process into a network of disease agents. We exemplify how the adaptive algorithm can be further exploited and used to model each individual in the network and their connections to other in a more realistic way.

Jimmy Calvo Monge
August 2023

CHAPTER 1

A nonlinear relapse model with disaggregated contact rates

Throughout the progress of epidemic scenarios it is expected to have different average daily contact behavior for individuals that are at different health classes. This contact heterogeneity has been studied in recent adaptive models and it allows to better captures the inherent differences across health statuses. Diseases with reinfection bring out more complex scenarios and they offer an important application in which to consider contact disaggregation. Therefore, we developed a nonlinear differential equation model to explore the dynamics of relapse phenomena and contact differences across health statuses. Our incidence rate function is formulated, taking inspiration from recent adaptive algorithms. It incorporates contact behavior for individuals in each health class. We use constant contact rates at each health status for our analytical results and prove conditions for different forward-backward bifurcation scenarios. The relationship between the different contact rates heavily influences these conditions. Numerical examples highlight the effect of temporarily recovered individuals and initial conditions on infected population persistence. The contents of this chapter can be read in the article [7].

---

1. Introduction

Epidemiological models serve as an essential tool for understanding disease dynamics. Many historical examples yield insightful results on how initial conditions and parameters alter the progression of an epidemic outbreak [4]; critical concepts developed in this setting, such as the R_0 reproductive number, work as threshold indicators for disease behavior. Modern epidemiological mathematics heavily use bread-and-butter SIR models [1], and current research efforts in this area are devoted to modifying the classical models, allowing them to capture all the intricacies of real-world disease dynamics, for example, better representation of social distancing phenomena, compliance conducts, economic conditions and other factors.

One effort in this area is related to studying human contact behavior. Contacts between individuals of different characteristics (health statuses, age groups ...) constitute a key factor in disease spread [45, 27, 9]. The need to study contact differences due to health status requires that classical models be modified. In classical settings, there is an implicit assumption of homogeneous behavior in each compartment (for example, among susceptible and infected individuals) through establishing constant or proportional contact rates. This approach hides different individuals' inherent characteristics and responses toward the disease's progress.

We now have a history of multiple efforts to deal with this problem. A first approach consists of specifying non-linear incidence rate functions by constructing functions that reflect the impact of

the state of the model on the contact rates through time; for example, [23, 24, 43, 21, 20, 25] for models without relapse, and [32, 44] for models with non-linear relapse rates. In these cases, the general idea is to include functions of the form

$$g_{\kappa,\nu}(\cdot)I = \frac{\kappa I^p}{1+\nu I^q},$$

as the incidence rate function for the disease, using positive constants κ, ν, p, q and with $I = I(t)$ the infected population size in time. Within relapse phenomena, very similarly, [32] proposes the function

$$g_{\kappa,\nu}(\cdot) = \frac{\kappa}{1+\nu\frac{R}{N}}, \tag{1.1}$$

where $R = R(t)$ is the number of (temporarily) recovered individuals at time t, and N is the total population size. As we can see, with this approach, modelers usually specify functions that decrease when the epidemic burden is high. This makes them depend inversely on the sizes of infected or recovered populations in time. The subsequent analysis is commonly focused on the impact of the model hyper-parameters (constants such as κ, ν in the non-linear functions) on the system behavior.

Key analytical results can be obtained using this approach. They can tackle the problem of different behaviors among health classes: what we call the *epidemiological heterogeneity* of agents involved in the disease progression. As mentioned in [16], although these models are rich in dynamic and analytical properties, the exact contact dynamic behavior sometimes is not emphasized in their formulation. In recent years new interest has been placed in representing more dynamic information on contact rates from the study population. Particularly, there has been interest in the *economical heterogeneity* of individuals involved in epidemics and in the inclusion of utilitarian adaptive decisions individuals make within the development of the epidemic scenario.

The main contribution from [15] consists of devising a process in which contact rates for individuals in each health class can be updated simultaneously as disease changes. The idea consists of modeling the individuals as decision agents who consider their environment status and utility to decide optimal contact rates throughout time. This approach considers individuals' economic considerations when deciding how many contacts they should engage with at each time period. A detailed review of other proposals under the epi-economical approach is available in [16].

This recent technique allows the computation of contact rates alongside the progress of the disease through an optimization decision process performed by each individual. We call this procedure the *adaptive setting*. This has proved helpful in creating epidemiological models closer to the actual decision-making processes made by individuals. It has been applied to create more realistic settings and compare them with the classical formulation. For example, thanks to the use of the adaptive setting, there are novel insights on the true impact of asymptomatic individuals [12], a more intuitive understanding of final epidemic burden states in contrast to the classical results [13], and a deeper analysis on social distancing [40]. Analytical comparisons and conjectures for the adaptive setting can be found under the non-relapse case in [26].

The adaptive setting is not detached from the first approach. To compute contact rates adaptively, we must first define non-linear incidence rate functions that will use these contact rates. The

formulation of non-linear incidence rate functions in the adaptive setting is commonly expressed in the form:

$$g(S,I,R) = \frac{C^s C^i N}{SC^s + IC^i + RC^r}, \tag{1.2}$$

where $C^h = C^h(S,I,R)$ (for $h \in \{s,i,r\}$) is the average number of contacts for each health status individual per time period, and N is the total population size. These contact rates might be functions that depend on the status of the disease S, I, R, especially when using the adaptive approach, where they are updated throughout the disease dynamics.

This adaptive setting constitutes a recent effort and offers a promising strategy to capture complex epi-economical phenomena better. Given its novelty, the literature on adaptive behavior has not been applied to non-linear relapse scenarios. Although several references propose non-linear relapse incidence rate functions for epidemiological differential equation models, the formulation (1.2) merits further analytical inspection in the relapse scenario. This paper uses this formula for incidence rate functions to study a relapse model. We will examine the analytical impact of specifying contact rates using (1.2) and the repercussions on how to interpret these models. Our results will be framed in terms of the relations between the contact rates C^s, C^i, and C^r when they are assumed constant. In Section 2, we propose our model and explore its main analytical properties. We present our main theoretical results in Section 3, where bifurcation plots and local stability are considered; all mathematical proofs can be found in Section 5. Section 4 provides some numerical simulations of sensitivity to contact rates and initial conditions. A discussion of our main results can be found in Section 5.

2. Non-linear relapse rate model

We propose an epidemiological model with the presence of non-linear relapse behavior. Following [38] and [39], we consider three compartments of individuals: S (susceptible), I (infected), and R (recovered with the possibility of reinfection) and represent the model dynamics using the following system of equations,

$$\begin{aligned} \frac{dS}{dt} &= -g(\cdot)\beta\frac{SI}{N} + \mu N - \mu S, \\ \frac{dI}{dt} &= g(\cdot)\beta\frac{SI}{N} + \phi\frac{RI}{N} - (\gamma+\mu)I, \\ \frac{dR}{dt} &= \gamma I - \phi\frac{IR}{N} - \mu R. \end{aligned} \tag{2.1}$$

$N = S + I + R$ is constant. The function $g(\cdot)$ is the incidence rate function of the model. From now on, we will take $g(\cdot)$ given by (1.2). This is the proposed relaxation of the burden of health status homogeneity, present in the classical formulation. The likelihood of infection when there is contact with an infected individual is given by β, the rate of recovery by γ, and the rate of reinfection represented by ϕ. We have a demographic exit and entrance rate for the system given by μ. The incidence rate function, $g(\cdot)$, represents the contact rate between susceptible and infected individuals, implying that $g(\cdot)\beta$ acts as the rate at which susceptible become infected.

We re-scale the system (2.1) by substituting $s := \frac{S}{N}, i := \frac{I}{N}$ and $r := \frac{R}{N}$, to obtain the equivalent model

$$\frac{ds}{dt} = -g(\cdot)\beta si + \mu - \mu s. \tag{2.2a}$$

$$\frac{di}{dt} = g(\cdot)\beta si + \phi ri - (\gamma + \mu)i. \tag{2.2b}$$

$$\frac{dr}{dt} = \gamma i - \phi ri - \mu r. \tag{2.2c}$$

The incidence rate function $g(\cdot)$ can also be re-scaled and substituted by:

$$g(\cdot) = g(s, i, r) = \frac{C^s C^i}{sC^s + iC^i + rC^r}.$$

Remark 2.1. In general, contact rates are functions that depend on the status of the disease, that is $C^h = C^h(S, I, R)$ for each $h \in \{s, i, r\}$. For the remainder of this article, we consider these functions constant. We aim to generalize mathematical results obtained in [32] and elucidate possible analytical properties of the adaptive algorithm in the relapse case. In this case, our mathematical analysis, including the calculation of R_0 and the determination of stable equilibria, will be greatly simplified. As will be seen shortly, all our results are greatly influenced by the ratios between the contact rates C^h.

3. Mathematical Analysis

3.1. **Basic Reproductive Number.** Using the next generation matrix approach [19], we compute a basic reproductive number R_0 for this system. Here, it is simple to see that

$$R_0 = \frac{\beta}{\gamma + \mu} \lim_{(s,i,r)\to(1,0,0)} g(s, i, r) = \frac{\beta}{\gamma + \mu} C_0.$$

Thus, R_0 depends on C_0, the limit of the incidence function value when the system converges to the disease-free state. When all contact coefficients C^h are constant, then $C_0 = C^i$.

3.2. **Finding equilibrium points.** First, we study the disease-free equilibrium, where $(s(t), i(t), r(t)) = (1, 0, 0)$.

Theorem 3.1. *The disease-free equilibrium is stable if and only if $R_0 < 1$.*

Proof. Note that the Jacobian matrix of the system (2.2) is given by

$$J(s, i, r) = \begin{pmatrix} -\beta i(g_s s + g) - \mu & -\beta s(g_i i + g) & -\beta s i g_r \\ \beta i(g_s s + g) & \beta s(g_i i + g) + \phi r - (\mu + \gamma) & \beta s i g_r + \phi i \\ 0 & \gamma - \phi r & -\phi i - \mu \end{pmatrix},$$

where g_h is the partial derivative of g with respect to the variable $h \in \{s, i, r\}$. Taking the limit to the disease-free point, we get

$$\lim_{(s,i,r)\to(1,0,0)} J(s, i, r) = \begin{pmatrix} -\mu & -\beta C_0 & 0 \\ 0 & \beta C_0 - (\mu + \gamma) & 0 \\ 0 & \gamma & -\mu \end{pmatrix},$$

which has eigenvalues $\lambda_1, \lambda_2 = -\mu$ and $\lambda_3 = \beta C_0 - (\mu + \gamma)$. This point is stable if and only if $\lambda_3 < 0$, which is equivalent to $R_0 < 1$. □

The case of epidemiological interest is when $R_0 > 1$, in which we study the existence of endemic equilibria. Initial calculations show that these points must be in the form $\left(1 - i^* - \frac{\gamma i^*}{\phi i^* + \mu}, i^*, \frac{\gamma i^*}{\phi i^* + \mu}\right)$. To find the value of i^* at the equilibrium, we can substitute this point into (2.2b), use that $r = 1 - s - i$ (as N is constant in this model) and obtain that i^* must satisfy the cubic equation $a_3X^3 + a_2X^2 + a_1X + a_0 = 0$, whose coefficients are:

$$
\begin{aligned}
a_3 &= R_\phi^2 R_0 - R_\mu R_\phi^2 \left(1 - \kappa\right), \\
a_2 &= R_\phi \Big[R_0(1 - R_\phi) + R_\mu(R_0 + R_\phi) - R_\mu(1 - R_\mu)\left(1 - \theta\right) - R_\mu(1 + R_\mu)\left(1 - \kappa\right) \Big], \\
a_1 &= R_\mu \Big[R_0(1 - R_\phi) + R_\phi(1 - R_0) - \left(1 - R_\mu\right)\left(1 - \theta\right) + R_\mu R_\phi - R_\mu \left(1 - \kappa\right) \Big], \\
a_0 &= R_\mu^2(1 - R_0), \qquad (3.1)
\end{aligned}
$$

where

$$
\kappa = \frac{C^i}{C^s}, \quad \theta = \frac{C^r}{C^s}, \quad R_\mu = \frac{\mu}{\mu + \gamma}, \quad R_\phi = \frac{\phi}{\mu + \gamma}. \qquad (3.2)
$$

Mathematically, the model proposed in [32] can be seen as a special case of our model: if we use $C^s = C^i$ and $C^r = C^i(1 + \nu)$, we obtain $g(\cdot)$ given by (1.1). This cubic equation also becomes the generalization of the corresponding one obtained in [32]. We also point out the biological interpretation of these contact quotients: κ represents the change expected in contacts made by an individual after it becomes infected, and θ compares the difference between the individual contacts before infection and after recovery.

We proceed to examine the behavior and existence of equilibria points based only on the disease parameters of the model (R_ϕ, R_μ), the infected individual response to the disease (R_0), and the relationship between the average contact rates between compartments ($\frac{C^i}{C^s}$ and $\frac{C^r}{C^s}$). In Figure (1) we use $\mu = 0.00015, \gamma = 0.0027, \beta = 0.00096$ and $\phi = 0.044$, taken from simulations made in [32] and drug epidemic parameter estimation performed in [39]. We create bifurcation plots for each R_0 and varying the quotients $\kappa = \frac{C^i}{C^s}$ and $\theta = \frac{C^r}{C^s}$. First, see Figure (1) for $\theta = 1.7$.

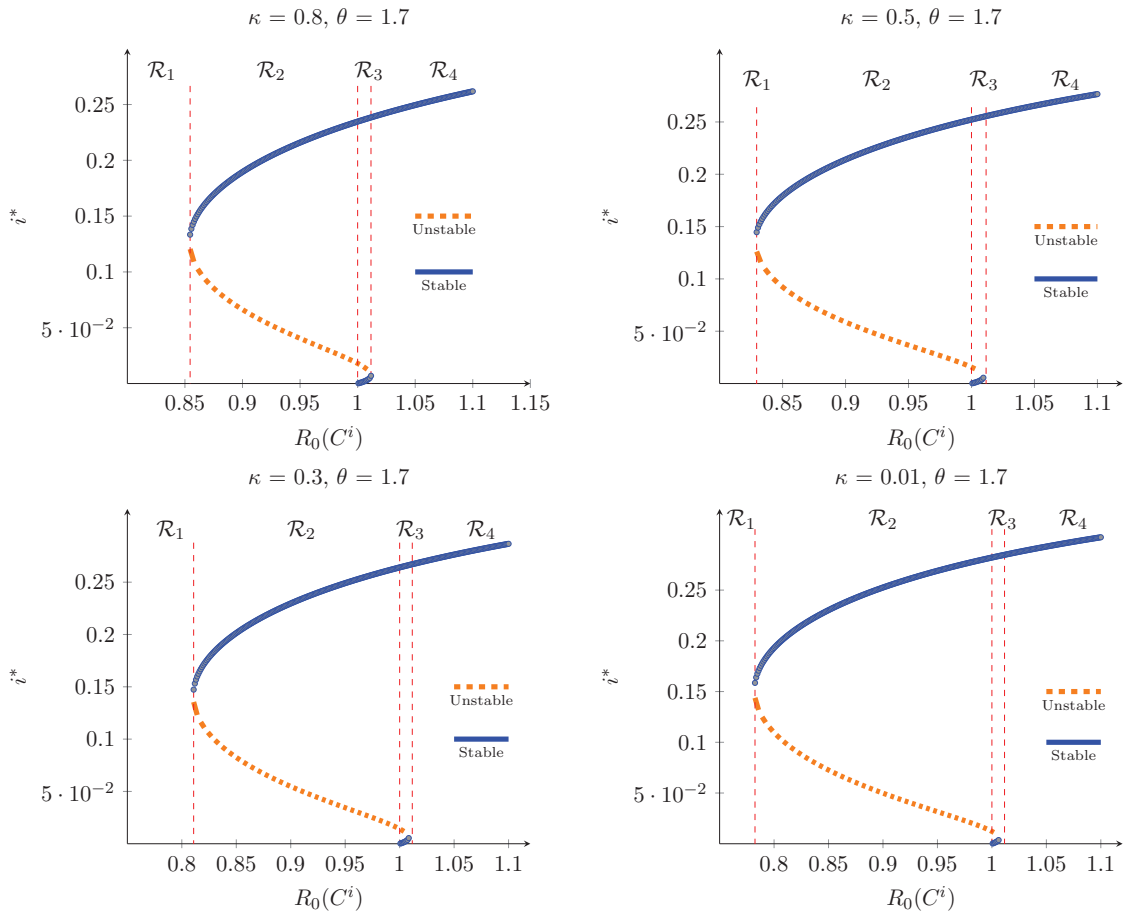

FIGURE 1. Equilibria points for the disaggregated model, computed using $\theta = 1.7$ and varying $\kappa = 0.8, 0.5, 0.3$ and 0.01.

A cubic bifurcation plot can be found, and three equilibria points occur within an interval $R_0 \in [1, 1 + \epsilon(\kappa, \theta)]$. We note that decreasing the value of κ diminishes the window $\epsilon(\kappa, \theta)$, and it decreases the minimal R_0 value for which we find stable equilibria, for example, for $\kappa = 0.8$ this value is at $R_0 \approx 0.85$, but for $\kappa = 0.01$ it is at $R_0 \approx 0.8$. For a discussion on the length of the window $\epsilon(\kappa, \theta)$, refer to Figure 6 below. Stable and unstable equilibria regions are highlighted in these plots.

We divided these plots into four regions of interest for the basic reproductive number: $\mathcal{R}_1$ where no endemic equilibrium is attained, $\mathcal{R}_2$ where a stable endemic equilibrium, and another non-stable can be found, $\mathcal{R}_3$ where three possible equilibrium states can be found, one of which is stable, and $\mathcal{R}_4$ where there is just one stable, steady state.

Remark 3.2. The presence of this cubic phenomenon was first observed in [32]. This case is of particular interest when analyzing the effect of the value of R_0 in epidemics with relapse. The small region in the $[1, 1+\epsilon(\kappa, \theta)]$ interval represents the possibility of having a very small stable equilibrium state of the disease even when the reproductive number is higher than 1. These simulations suggest the importance of the contact rate C^r in creating such a scenario.

On the other hand, decreasing the value of θ leads to a different behavior, as shown in Figure (2). In this case, we count three regions of interest exhibiting a typical backward quadratic bifurcation plot. We can see that no R_0 allows us to obtain three possible equilibria points.

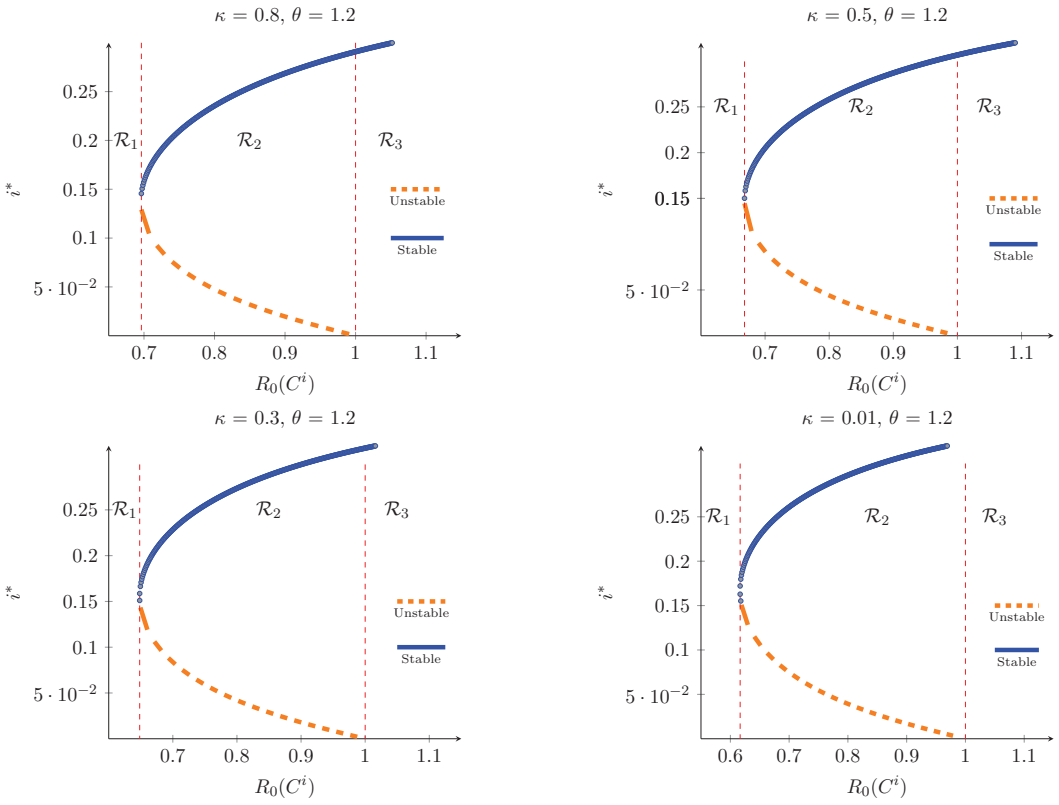

FIGURE 2. Equilibria points for the disaggregated model, computed using $\theta = 1.2$ and we varying $\kappa = 0.8, 0.5, 0.3$ and 0.

Remark 3.3. From the previous numerical results, we can derive the following conjectures:

a) A cubic bifurcation plot can be found for sufficiently high values of $\theta = \frac{C^r}{C^s}$, independently of κ. We observe an interval for R_0 in which those three equilibria points can be found, and it depends on (θ, κ).
b) For cubic bifurcation plots, a sensible region $[1, 1 + \epsilon]$ could attain an endemic stable or a small non-stable equilibrium.
c) When θ is small, there is no cubic behavior for any κ, and for all $R_0 > 1$, there is only one possibility for an endemic equilibrium.

3.3. **Theoretical Results.** Based on our previous simulations, we would like to formalize the conditions for the existence of regions that provide us with such cubic behavior. For that, we propose the following result.

Theorem 3.4. *Let μ, γ, ϕ be positive real numbers. Define R_μ and R_ϕ as in (3.2) and suppose that*

$$R_\phi > \frac{1+R_\mu^2}{(1-R_\mu)^2}. \tag{3.3}$$

Then, there exist $0 < \theta_1 < \theta_2$ such that for every $\theta \in [\theta_1, \theta_2]$ and every $\kappa \in [0,1]$, there is an $R_0 > 0$ such that the polynomial equation $a_0 + a_1 X + a_2 X^2 + a_3 X^3 = 0$ where $a_0, \cdots, a_3$ are defined by (3.1), has three distinct real roots in the interval $[0,1]$. Moreover, for each pair (κ, θ), this hold for all R_0 in a neighborhood of the form $[1, 1+\epsilon(\theta)]$.

In other words, there is a range of the fraction $\theta = \frac{C^r}{C^s}$ which yields a cubic bifurcation plot, under our condition (3.3), independently of the value of $\kappa = \frac{C^i}{C^s}$. We present the proof of this theorem, which uses the algebraic theory of Sturm chains. A preamble for this theory can be found in the Appendix.

Proof. Let us assume that the polynomial $f(X)$ has three different real roots. In this case, as discussed in proposition (5.6), the sequence of higher derivatives of $f(X)$ forms a Sturm sequence on any interval. This sequence is then

$$[a_0 + a_1 X + a_2 X^2 + a_3 X^3, a_1 + 2a_2 X + 3a_3 X^2, 2a_2 + 6a_3 X, 6a_3].$$

Its values at $x = 0$ and $x = 1$ are respectively $(a_0, a_1, 2a_2, 6a_3)$ and $(a_0 + a_1 + a_2 + a_3, a_1 + 2a_2 + 3a_3, 2a_2 + 6a_3, 6a_3)$. Our goal will be to find values for R_0 for which the signs of these sequences are $-, +, -, +$ at $x = 0$ and $+, +, +, +$ at $x = 1$. By Proposition (5.6), this would prove the existence of three different roots in the interval $[0,1]$, since in this case $V_S(0) = 3$ and $V_S(1) = 0$. The reader can verify that for this to happen it is enough to have:

$$a_0 < 0, \quad a_2 < 0, \quad a_3 > 0, \quad a_0 + a_1 > 0, \quad \text{and } a_2 + a_3 > 0. \tag{3.4}$$

Note that if $R_0 > 1$ then $a_0 < 0$ and if $R_0 > R_\mu$, then for all $\kappa \in [0,1]$ we have

$$a_3 = R_\phi^2[R_0 - R_\mu(1-\kappa)] > R_\phi^2[R_0 - R_\mu] > 0.$$

Because $R_\mu < 1$, then $R_0 > 1$ is sufficient to ensure that $a_0 < 0$ and $a_3 > 0$.

We now move to a coordinate plane with R_0 in the x-axis and θ in the y-axis. The coefficients $a_0, \ldots, a_3$ can be seen as linear equations in this plane, given by

$$\begin{aligned} a_3 &= AR_0 - B(1-\kappa) \\ a_2 &= C + DR_0 - E(1-\kappa) - F(1-\theta) \\ a_1 &= G + HR_0 - I(1-\kappa) - J(1-\theta) \\ a_0 &= K(1-R_0), \end{aligned}$$

where the constants $A, B, \cdots, K$ depend only on R_ϕ and R_μ and are given by

$$A := R_\phi^2, \quad B := R_\mu R_\phi^2, \quad C := R_\phi^2 R_\mu, \quad D := R_\phi(1 - R_\phi) + R_\phi R_\mu,$$
$$E := R_\phi R_\mu(1 + R_\mu), \quad F := R_\phi R_\mu(1 - R_\mu), \quad G := R_\phi R_\mu(1 + R_\mu)$$
$$H := R_\mu(1 - R_\phi) - R_\mu R_\phi, \quad I := R_\mu^2, \quad J := R_\mu(1 - R_\mu) \quad K := R_\mu^2.$$

Note that all constants are positive, except perhaps D and H (we don't know the sign of $1 - R_\phi$).

Geometrically, the inequalities in (3.4) refer to an area that is below the line $\ell_1 := \{a_2 = 0\}$ and above the lines $\ell_2 := \{a_2 + a_3 = 0\}$ and $\ell_3 := \{a_0 + a_1 = 0\}$ in the (R_0, θ) plane. Consider the intersections of these three lines with the $R_0 = 1$ vertical line. If we prove that the θ coordinate of the intersection of the ℓ_1 with this vertical axis is bigger than the θ coordinates of intersections of the other two (ℓ_2 and ℓ_3), then there would be an interval to the right of $R_0 = 1$ which is below the line ℓ_1 and above both ℓ_1 and ℓ_3. See the next figure for a visual intuition.

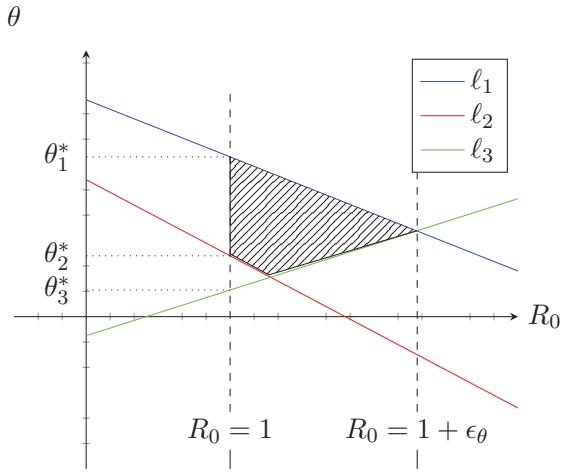

FIGURE 3. Intuition behind the proof of theorem 3.4

This is a specific example, and we don't know the signs of the slopes of lines ℓ_1, ℓ_2, and ℓ_3. However, their intersections at $R_0 = 1$ define the existence of a region below ℓ_1 and above both ℓ_2 and ℓ_3 in a neighborhood of $R_0 = 1$.

The intersection of line ℓ_1 at $R_0 = 1$ gives us

$$\theta_1^* = 1 - \frac{C + D}{F} + \frac{E}{F}(1 - \kappa),$$

and the intersection of line ℓ_2 at $R_0 = 1$ gives us

$$\theta_2^* = 1 - \frac{C + D}{F} + \frac{E}{F}(1 - \kappa) + \frac{B(1 - \kappa) - A}{F} < \theta_1^* + \frac{B - A}{F},$$

we note that $B - A = R_\mu R_\phi^2 - R_\phi^2 = R_\phi^2(R_\mu - 1) < 0$, so we indeed have $\theta_2^* < \theta_1^*$.

The θ coordinate of the intersection between ℓ_3 and $R_0 = 1$ is

$$\theta_3^* = 1 - \frac{G + H}{J} + \frac{I}{J}(1 - \kappa) < 1 - \frac{G + H}{J} + \frac{I}{J}.$$

We observe that $\theta_1^* > 1 - \frac{C+D}{F}$ for all $\kappa \in [0,1]$, so we would need

$$1 - \frac{C+D}{F} > 1 - \frac{G+H}{J} + \frac{I}{J},$$

to guarantee $\theta_3^* < \theta_1^*$ for all κ. This is equivalent to $(G+H-I)F > (C+D)J$, and by expanding this expression, we get the inequality (3.3) from our statement. Note that this region can be obtained independently of κ. Inequality (3.3) will imply that $\frac{C+D}{F} < 1$ and $\frac{G+H-I}{J} < 1$, and these are readily seen to imply that $\theta_i^* > 0$ for $i = 1, 3$. Therefore the desired interval for θ can be taken between $\max\{\theta_3^*, \theta_2^*\}$ and θ_1^*.

This proves that when (3.3) is true, and our polynomial $f(X)$ doesn't have repeated roots, there is a region in the (R_0, θ) plane for which $f(X)$ has three real distinct roots in the interval $[0,1]$. □

Remark 3.5. We note that both R_0 and the coefficients $a_0, \cdots, a_3$ are dependent, simultaneously, on the values of C^h. If we fix the values of κ and θ, all results will depend only on one of the C^h's.

In the next section, we will explore numerical results related to this theorem. Our examples concern the $C^i < C^s$ scenario ($\kappa < 1$). In this case, we assume that infection decreases contacts, which is intuitive. The other option, $\kappa > 1$, makes biological sense when infected populations are large because, under those circumstances, susceptible individuals may be overly cautious about engaging in contact with others [26]. The following theorem shows that the case $\kappa > 1$ is more stable. Because of this, we focus on the $\kappa < 1$ scenario from now on.

Theorem 3.6. *If $C^i > C^s$ then (2.1) has no limit cycles in the region $\{(i,r) \in \mathbb{R}^2 : i > 0, r > 0\}$.*

Proof. We use a similar technique as in [3]. Writing $s = 1 - i - r$, we obtain the two-variable system:

$$\begin{aligned} \frac{di}{dt} &= g(1-i-r, i, r)\beta i(1-i-r) + \phi r i - (\gamma+\mu)i = g_1(i,r) \\ \frac{dr}{dt} &= \gamma i - \phi r i - \mu r = g_2(i,r). \end{aligned} \tag{3.5}$$

Then we have that

$$\begin{aligned} \frac{g_1(i,r)}{ir} &= g(1-i-r,i,r)\beta\left(\frac{1-i-r}{r}\right) + \phi - (\gamma+\mu)\frac{1}{r}, \\ \frac{g_2(i,r)}{ir} &= \frac{\gamma}{r} - \phi - \frac{\mu}{i}. \end{aligned}$$

This implies that

$$\begin{aligned} &\frac{\partial}{\partial i}\left(\frac{g_1(i,r)}{ir}\right) + \frac{\partial}{\partial r}\left(\frac{g_2(i,r)}{ir}\right) \\ &= \left[\left(\frac{\partial g}{\partial i} - \frac{\partial g}{\partial s}\right)\beta\left(\frac{1-i-r}{r}\right)\right] - \frac{\beta g(1-i-r,i,r)}{r} - \frac{\gamma}{r^2}. \end{aligned}$$

This is negative when $\frac{\partial g}{\partial i} - \frac{\partial g}{\partial s} < 0$, and using the definition of $g(\cdot)$ given by (1.2), this is equivalent to $C^s < C^i$. Applying the Dulac criterion, we obtain the non-existence of limit cycles in the region $\{(i, r) \in \mathbb{R}^2, i > 0, r > 0, i + r < 1\}$ for this system of differential equations. □

4. Numerical Results

4.1. **Stable equilibrium points.** We explore the equilibrium results in a simulation of disease scenarios. Let us consider Figure (1) with the case $\kappa = 0.8$ and $\theta = 1.7$ (and all the other model parameters as in that example). Using $C^i = 3$ we obtain $R_0 \approx 1.01057$. This R_0 is found in the $\mathcal{R}_3$ region in the bifurcation plot. Solving the corresponding cubic equation, we obtain three possible theoretical equilibrium points: $i^* \in \{i_1^* = 0.004914, i_2^* = 0.010455, i_3^* = 0.238099\}$.

Of these possibilities, i_3^* and i_1^* are asymptotically stable equilibrium points. The system could converge to each point depending on its initial conditions. The middle point, which is unstable, actually works as a threshold value as solutions drift away from it. If we take initial conditions $a_0 = (S(0), I(0), R(0))$ with $N = S(0)+I(0)+R(0)$, and let $i(0) = \frac{I(0)}{N}$, then the highest equilibrium will attract all solutions when $i(0) > i_2^*$, otherwise it is the lowest equilibrium to which the system converges.

The following graphs show cases for convergence to each equilibrium point. Figure (4) displays $i(t)$ through time using initial conditions $a_0 = (N-\rho N-10, \rho N, 10)$, where $\rho \in [0, 1]$ and $N = 10000$. On the left are some simulations using $\rho > i_2^*$, in which the system converges to i_3^*, the highest equilibrium possible. On the right, a system is solved with $\rho < i_2^*$, where the final point obtained is i_1^*, although with a much slower convergence rate. We included the bifurcation plot on the left, highlighting the region of interest.

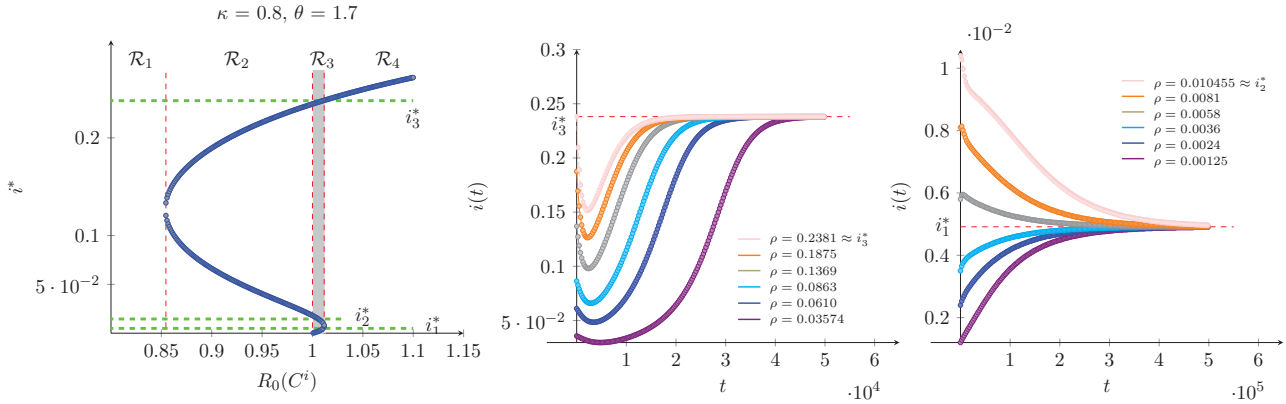

Figure 4. Convergence of $i(t)$ to the equilibrium point i^*, for the disaggregated model.

On the left, the bifurcation plot was obtained for this case, with region $\mathcal{R}_3$ highlighted. The center plot shows cases of convergence to the maximum possible equilibrium point within this region. This happens when the initially infected proportion is high enough. The plot on the right shows cases of convergence towards the smallest equilibrium point in this region, obtained for sufficiently small values of $i(0)$.

4.2. **Effect of** (κ, θ)**.** Now we explore how the values of κ and θ affect the size of the final equilibrium points [1]. To compare within a given R_0, we fix $C^i = 3$ (thus obtaining $R_0(C^i)$ as the examples above) and vary the values of C^s and C^r using κ and θ respectively, we set $\kappa \in [0, 1]$ and $\theta \in [0, 2]$. Figure (5) shows the effect of increasing both values on the stable steady states attained in the model for two different initial conditions. We observe that increasing κ or θ yields a reduction in the final equilibrium of the system. However, we note that the value of this state is more sensible to θ than κ, indicating that, in the relapse case, contacts made by recovered individuals have a stronger impact on the disease outcome. Furthermore, we can see that high values of (κ, θ) may induce the system to attain a semi-disease-free steady state. This state, naturally, is more likely to be obtained when $i(0)$ is small, as seen by comparing both cases in Figure (5). In other words, a considerable infected population makes this population more likely to become established.

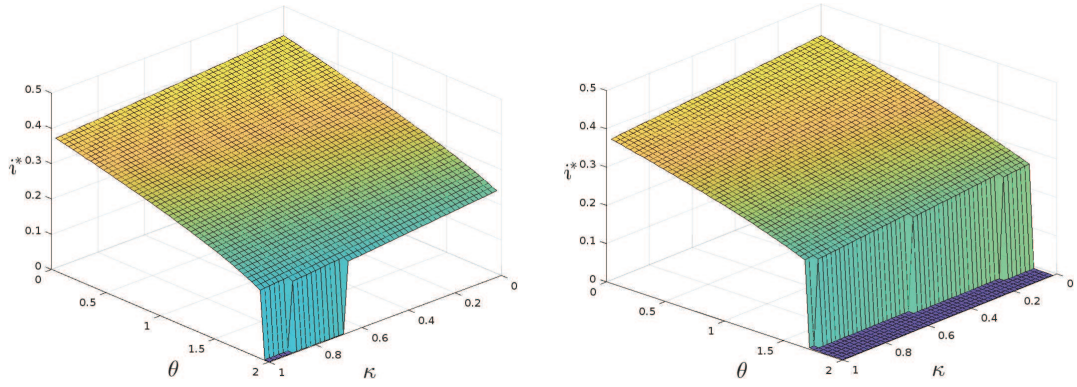

FIGURE 5. Effect of (κ, θ) for two different initial condition scenarios.

On the left using $i(0) = 0.1$, on the right $i(0) = 0.02$. For low initial infected populations, a high value of θ yields disease eradication, independently of κ.

Region $\mathcal{R}_3$ offers the most interesting behavior. In other regions, the disease is either maintained at a high steady prevalence or eradicated. In region $\mathcal{R}_3$, there is the possibility of a low equilibrium state, without achieving the disease disappearance from the population. However, the window for this behavior is small. For $\theta > \theta_1$ (as in Theorem 3.4), we find a window $[1, R_{0,\max}(\kappa, \theta)]$ which defines region $\mathcal{R}_3$, the next figure shows the upper limit of this interval, depending on (κ, θ). We can again infer a similar situation. This window becomes larger when $||(\theta, \kappa)||$ increases, however, the effect of θ is more prominent. In this case, $\theta_1 \approx 1.4$.

[1]For each point on the grid, the convergence speed of the system varies. Each simulation was performed at a point in time when the difference between successive time states fell below a machine precision threshold.

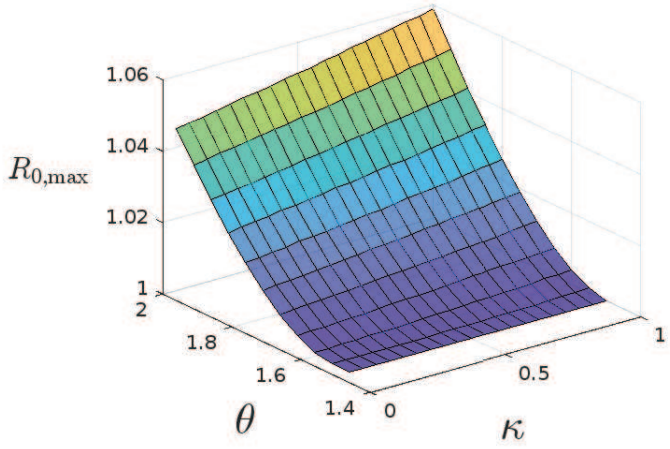

FIGURE 6. Effect of (κ, θ) on the $\mathcal{R}_3$ window length.

When θ increases, there is more room to observe this region with more unstable behavior.

Remark 4.1. Note that in these simulations, we decided to place less focus on the disease parameter β. The reason for this lies in the scale of the incidence rate function $g(\cdot)$. By using contact rates $C^i = 3$ and $C^s = C^i/\kappa, C^r = C^i/\theta$, the scale forces us to reduce the value of β to work with incidence rates that produce valuable epidemic scenarios. For example, if we use $\beta = 0.0096$, as in [32, 39], this scenario would give us a basic reproductive number of $R_0 \simeq 10.105$ using these contacts, an exceedingly high and unrealistic number in many applications, which brings the model to a biological scenario with a single stable equilibrium point, resulting of an overestimation of the incidence term $\beta g(\cdot)SI/N$ of the system. Therefore, we note the importance of keeping in mind the scales of incidence rate functions when using the contact information in incidence rate functions for these models.

4.3. **Other Examples.** In this subsection, we consider some numerical results and discussions on possible extensions of the contact rate disaggregation approach taken in the present study.

Example 4.2 (Disaggregated contacts for Influenza, a non-relapse case)**.** We study the effect of disaggregated contact rates in epidemics models for individual-based transmitted diseases such as influenza. In this example, we use parameters for influenza transmission based on estimations performed in [8] [2]. We then consider model 2.1 with the following epidemic parameters.

- $\beta = 0.07943065$,
- $\gamma = 0.243902 = 1/4.1$ (equivalent to 4.1 recovery period as mentioned in [8]),
- $\phi = 0$, and $\mu = 0.0005$.

The estimation of the β infection parameter was performed as follows. For influenza, [8] obtains a natural reproduction number estimation, $R_p \simeq 1.3$ for influenza seasons in different countries from

[2]Other parameters can be obtained also from [17].

1972-1997. The number R_p is defined as $R_p := R_0(1-p)$ where p is assumed to be a proportion of susceptible individuals that have been successfully immunized before an epidemic. We perform simulations with R_0 obtained using $p = 0.2$, and $C^i = 5$, giving $R_0 \approx 1.625$.

Although this model presents a non-relapse scenario, we can still incorporate the contact information and obtain similar numerical results as before. For example, as observed in Figure 7, the effect of θ over the peak epidemic prevalence of the model seems to be stronger than the effect of κ, thus indicating a similar behavior in the non-relapse case in terms of the contact proportions κ, θ. In this non-relapse scenario, our focus shifts towards the peak prevalence, as the final equilibrium will have a null infected population.

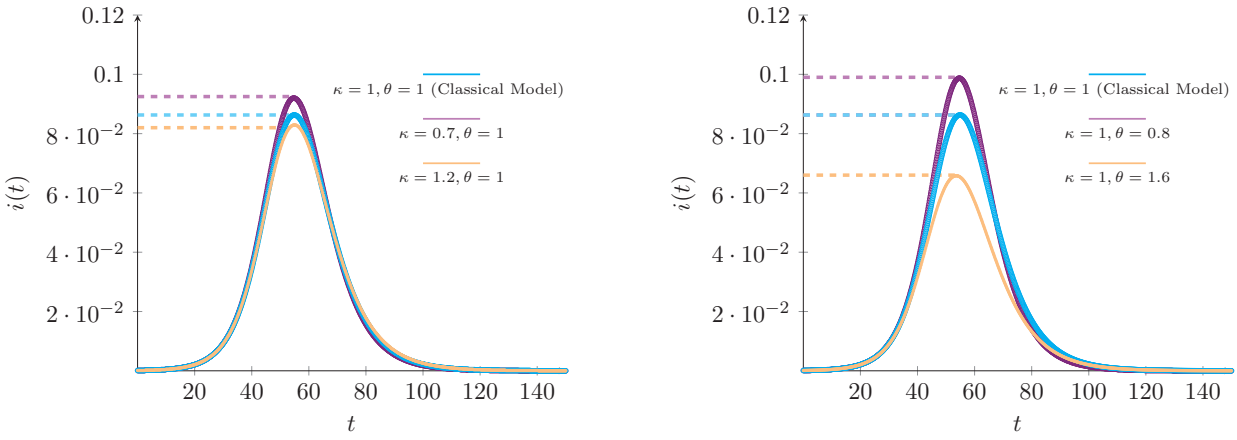

FIGURE 7. Different infected results varying both contact proportions κ and θ.

We keep $\theta = 1$ on the left and vary the proportion κ. Conversely, we keep $\kappa = 1$ on the right and vary the value of θ. We observe a bigger effect on the peak prevalence obtained in the figure on the right, that is, varying θ.

We expand these results for several combinations of values for (κ, θ) in the surface plot in Figure (8). We obtain a parallel situation as in the relapse simulations: we observe a bigger slope in the θ axis than in the κ axis.

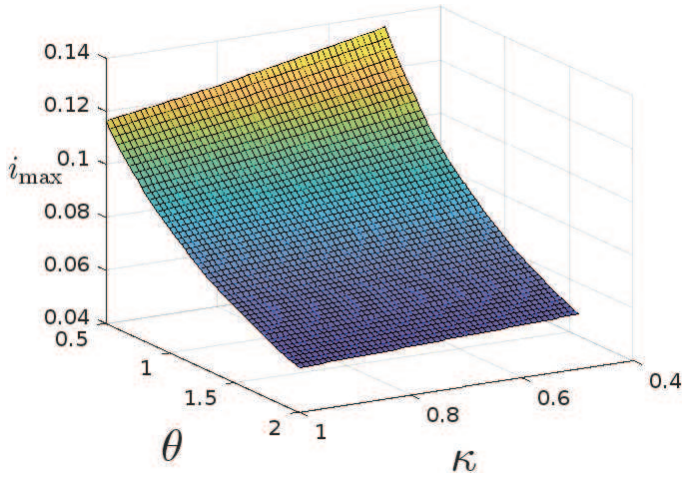

FIGURE 8. Disease peak infected prevalence varying both contact proportions κ and θ for the influenza simulation example.

We note that, in general, a reduction in peak prevalence is expected using the disaggregated contact rates in comparison to the classical SIR model. For the non-relapse case, this was pointed out within simulations performed in [15] and also expanded by the results of this example; for the non-relapse case this observation has been supported by our simulations in the previous sections.

Example 4.3 (Disaggregated contacts approach for more complex models: Discussion)**.** Incidence rate functions control the entrance of susceptible individuals into the infected population. In the classical SIR model, this occurs because of contact with other infected individuals. This is reflected in the numerator of the incidence rate function, being $C^s C^i N$, consisting of the susceptible contacts multiplied by the contribution of infected contacts[3]. The denominator constitutes the total population activity, given by $\sum_h C^h h$, where the sum is over all possible health statuses, this yields the incidence rate as a proportion of the contact activity of the infected in terms of the total contact activity.

When adding new compartments or modifying the formulation of the model and trying to use the disaggregated contact approach discussed in the present study, this incidence rate formula should follow the same pattern: for the numerator to consider the contact information of compartments that might cause infection to susceptible individuals, and the denominator to reflect the total activity. We discuss some cases of how to apply this method to introduce such functions into more general epidemiological models.

First, consider the model proposed in [13]. Here, the authors provide a modified SIR model of risk-taker (S_1) and risk-evader (S_2) susceptible to study COVID-19 epidemic scenarios. This non-relapse epidemic model was fitted using the adaptive approach, which implies the use of contact-disaggregated incidence rate functions. For each group of susceptible, the infection might come

[3]We could also argue that a better formulation for this denominator would be $C^s C^i I$, by reducing the effect only to consider the volume of the infected population. Looking at equations 4.1, we see that [13] follows this idea. We decided instead to use the first formulation as it was the approach taken in the original adaptive setting reference: [15].

as a result of contact either with infectious exposed -both risk-takers and risk-evaders (E_1, E_2)-, infectious asymptomatic -both risk-takers and risk-evaders (A_1, A_2)- and infected symptomatic (I). Therefore, the incidence rate for both susceptible compartments is given by

$$
\begin{aligned}
g_1(\cdot) &:= C^{S_1} \frac{\rho(C^{E_1}E_1 + C^{E_2}E_2) + \alpha(C^{A_1}A_1 + C^{A_2}A_2) + C^I I}{\sum_h C^h h} \\
g_2(\cdot) &:= C^{S_2} \frac{\rho(C^{E_1}E_1 + C^{E_2}E_2) + \alpha(C^{A_1}A_1 + C^{A_2}A_2) + C^I I}{\sum_h C^h h},
\end{aligned} \tag{4.1}
$$

where $h \in \{S_1, S_2, E_1, E_2, A_1, A_2, I, R\}$ (the model also has a recovered compartment, naturally), $\epsilon \in (0, 1)$ is a reduction in infectious chances by taking a risk-evader approach, and ρ, α are reduction constants for non-symptomatic infectious populations. This example gives us an application of the abovementioned principle in constructing contact-based incidence rate functions.

Another interesting example of the application of this principle consists of vector-borne diseases. In these cases, susceptible humans become infected not by contact with other infected human individuals, but rather by contact with infected vectors. Furthermore, susceptible vectors become infected by contact with infected humans. This dynamic requests a change of form in the incidence rate functions. Let us take, for example, the dengue-chikungunya vector-borne epidemic model proposed in [33]. This model considers two populations: hosts (h) and vectors (v), and it is based on the following system of differential equations.

Hosts	Vectors
$\frac{dS_h}{dt} = \mu_h N_h - \beta g_h(\cdot) S_h \frac{I_v}{N_v} - \mu_h S_h$	$\frac{dS_v}{dt} = \mu_v N_v - \beta_v g_v(\cdot) S_v \frac{I_h}{N_h} - \mu_v S_v$
$\frac{dE_h}{dt} = \beta g_h(\cdot) S_h \frac{I_v}{N_v} - (\mu_h + \alpha_h) E_h$	$\frac{dE_v}{dt} = \beta g_v(\cdot) S_v \frac{I_h}{N_h} - (\mu_v + \alpha_v) E_v$
$\frac{dI_h}{dt} = \alpha_h E_h - (\mu_h + \gamma) I_h$	$\frac{dI_v}{dt} = \alpha_v E_v - \mu_v I_v$
$\frac{dR_h}{dt} = \gamma I_h - \mu_h R_h$	

Here, the host population has five health classes: S_h, susceptible hosts, E_h, exposed hosts, I_h, infected hosts, and R_h, recovered hosts, and the vector population has three: S_v, susceptible vectors, E_v, exposed/latent vectors, and I_v, infected vectors. Total populations are N_h for hosts and N_v for vectors. There are no recovered vectors, as they die with the disease. For each population, we inserted incidence rate functions $g_h(\cdot), g_v(\cdot)$, which are constant and equal to 1 in [33].

Following the abovementioned principle, we can propose the following formulas for both functions.

$$
\begin{aligned}
g_h(\cdot) &:= \frac{C^{S_h} C^{I_v} I_v}{\sum_j C^j j} \\
g_v(\cdot) &:= \frac{C^{S_v} C^{I_h} I_h}{\sum_j C^j h},
\end{aligned} \tag{4.2}
$$

where $j \in \{S_h, E_h, I_h, R_h, S_v, E_v, I_v\}$ goes through all possible health statuses. This formulation considers the infection dynamics of vector-borne diseases: hosts become infected after contact with infected vectors, and vectors become infected after contact with infected hosts. Equations 4.2 offer an alternative for researching the possible impact of non-linear incidence rate functions in more

complex scenarios, such as vector-borne diseases. Introducing contact rates between susceptible hosts and infected vectors could offer a mathematical approach to model the interactions between these two populations and understand further indirect contact-impacting measures, such as protection against vectors. We believe this offers an opportunity to further understand the dynamics of this biological scenario, especially in light of real data-based analysis, such as performed in [33].

5. Discussion

Motivated by the recent advances in the adaptive setting framework, we proposed a model incorporating non-linear relapse and contact behavior among individuals of different health classes. Our study aimed to explore the analytical properties of this model and investigate the effects of disaggregating contact rates on disease dynamics. We found that the model exhibits a high sensitivity to initial conditions and the relationships between contact rates, with significant implications for disease control strategies.

To gain insights into the behavior of our model, we performed numerical simulations that revealed several important features. First, we observed that the model's dynamics are highly dependent on the values of the basic reproductive number (R_0), which reflects the behavior of infected individuals. We established explicit conditions for multiple stable infected populations, which are highly sensitive to the model's initial conditions. Furthermore, we found that the impact of the contact rates for recovered individuals with relapse (θ) is more substantial than that of infected individuals (κ), with larger differences required to achieve complete disease control for higher initial epidemic volumes.

Models incorporating relapse phenomena highlight the significant impact of recovered individuals on the progress of diseases. Such models exhibit different dynamics compared to those without relapse, with distinct results regarding recovery and relapse. Our study supports this view, with our conclusions showing that changes in the contact behavior of recovered individuals (θ) have a more substantial effect on epidemic equilibria than corresponding changes in contact rates for infected individuals (κ), after normalizing with respect to the susceptible contact rate. The differences in behavior when recovering from the disease (or addiction) play a crucial role in determining the prevalence of the disease. Our findings suggest that a low θ value, indicating a lack of meaningful contact engagement by recovered individuals after infection, can establish a considerable epidemic burden. This highlights the importance of successfully reintegrating recovered individuals into society, which can reduce the likelihood of significant epidemics. Similar conclusions regarding the impact of recovered individuals on bifurcation plots have been observed in other relapse models [41].

Our results are closely tied to the behavior of infected individuals, as captured by the basic reproductive number R_0. We established explicit conditions for the existence of a region $1 < R_0 < R_{0,\max}$, characterized by multiple stable infected populations, which are highly sensitive to the model's initial conditions. We also found that this region becomes wider as the contacts of recovered individuals with relapse increase. In our simulations, we observed that the impact of (κ, θ) is intertwined with the initial infected population size, with larger initial epidemic volumes requiring more significant differences in contact rates to achieve disease control.

Building on the mathematical analysis presented in [32], we confirmed the conclusions and discussions regarding the influence of recovered individuals on the prevalence of diseases with relapse.

Incorporating non-linear relapse significantly alters the dynamics of the SIR model, leading to more complex equilibria and bifurcation considerations. Our analysis adopted a non-linear relapse formulation (1.2) that assumes fixed contact rates among health compartments. We aimed to obtain analytical results that can be compared to future studies using a complete adaptive formulation. Such comparisons will be made against the non-linear non-adaptive model proposed in this article.

Our study underscores the importance of incorporating adaptive behavior and contact heterogeneity into epidemiological models, particularly in the presence of relapse phenomena. The results can inform public health policy decisions and provide a foundation for future research into the behavior of complex disease systems.

Appendix A: Sturm Theory

We use the general theory of Sturm chains to prove the theorem (3.4). Here we set some basic definitions and properties. We base this treatment on the theory detailed in [11].

Definition 5.1. A sequence $S = \{p_0(x), p_1(x), p_2(x), \cdots, p_n(x)\}$ of polynomials in $\mathbb{R}[x]$ is called a **Sturm chain** with respect to an interval I if it satisfies the Sturm property:

If $\alpha \in I$ is a real root of $p_i(x)$, for some i with $0 < i < n$. Then $p_{i-1}(\alpha)p_{i+1}(\alpha) < 0$.

Definition 5.2. Let f be a real rational function. The Cauchy index of f at x is defined by

$$\mathrm{Ind}_x(f) := \mathrm{Ind}_x^+(f) - \mathrm{Ind}_x^-(f), \quad \text{where for} \sigma \in \{+,-\} \text{we have}$$

$$\mathrm{Ind}_x^\sigma(f) := \begin{cases} +\frac{1}{2}, & \text{if } \lim\limits_{y \to x^\sigma} f(y) = +\infty, \\ -\frac{1}{2}, & \text{if } \lim\limits_{y \to x^\sigma} f(y) = -\infty, \\ 0, & \text{otherwise.} \end{cases}$$

The Cauchy index of f at $[a, b]$ is then given by

$$\mathrm{Ind}_a^b(f) := \mathrm{Ind}_a^+(f) - \mathrm{Ind}_b^-(f) + \sum_{x \in]a,b[} \mathrm{Ind}_x(f). \tag{5.1}$$

Remark 5.3. We can assume that f is in its reduced form. That is, the numerator and denominator have no common factors. In this case, $\mathrm{Ind}_x(f)$ is non-zero (with values 1 or -1) only for odd-multiplicity roots of the denominator, and since there are only finitely many such points, the sum in 5.1 is well defined.

We state the following generalization of the classical *Sturm Theorem.*

Theorem 5.4 ([11], Theorem 3.11)**.** *If $S = \{p_0(x), p_1(x), ..., p_{n-1}(x), p_n(x)\}$ is a Sturm chain in $\mathbb{R}[x]$ with respect to $[a, b]$, then*

$$\mathrm{Ind}_a^b\left(\frac{p_1}{p_0}\right) + \mathrm{Ind}_a^b\left(\frac{p_{n-1}}{p_n}\right) = V_S(a) - V_S(b). \tag{5.2}$$

Where $V_S(c)$ is the number of sign changes in the values of consecutive polynomials of the chain S at a point $x = c$; that is, the number of those $j \in \{1, \dots, n\}$ for which $p_{j-1}(c)p_j(c) < 0$.

This theorem can be applied to a special case of non-repeated roots, but first, we need the following auxiliary lemma, which standard calculus arguments can prove.

Lemma 5.5. *Let $p_0(x)$ be a polynomial of degree n with n distinct real roots. Suppose that $c \in \mathbb{R}$ such that $p'(c) = 0$, then $p(c)p''(c) < 0$.*

Proposition 5.6. *Let $p_0(x)$ be a polynomial of degree n that has n distinct real roots, then the sequence $S_0 = \{p_0(x), p_0'(x), p_0^{(2)}(x), p_0^{(3)}(x), \cdots, p_0^{(n)}(x)\}$ of higher derivatives of $p_0(x)$ is a Sturm chain with respect to any interval $[a, b]$. Moreover, if $p_0(a)p_0(b) \neq 0$, then the number of roots of $p_0(x)$ in $[a, b]$ equals $V_{S_0}(a) - V_{S_0}(b)$.*

Proof. By a repeated application of Lemma 5.5, it is easy to check that the sequence S_0 of higher derivatives of $p_0(x)$ is a Sturm chain with respect to any interval I. Given that $p_0^{(n)}$ is a non-null constant, then $\frac{p_0^{(n-1)}}{p_0^{(n)}}$ is a polynomial which means that $\mathrm{Ind}_a^b\left(\frac{p_0^{(n-1)}}{p_0^{(n)}}\right) = 0$. For the first term in 5.2, if we write $p_0(x) = c(x - a_1)\cdots(x - a_n)$, where $a_1, \dots a_n$ are the roots of p_0, we have

$$\frac{p_1(x)}{p_0(x)} = \frac{p_0'(x)}{p_0(x)} = \frac{c\sum_{i=1}^n \prod_{j\neq i}(x - a_j)}{c\prod_{j=1}^n (x - a_j)} = \frac{1}{x - a_1} + \frac{1}{x - a_2} + \dots \frac{1}{x - a_n}.$$

So, for each $j = 1, \dots, n$, $\lim_{x\to a_j^{\pm}} = \pm\infty$, that is $\mathrm{Ind}_{a_j}\left(\frac{p_0'}{p_0}\right) = 1$. Therefore, the Cauchy index $\mathrm{Ind}_a^b\left(\frac{p_0'}{p_0}\right)$ is the number of roots of p_0 that are contained in $[a, b]$, and by Theorem 5.4, this coincides with $V_{S_0}(a) - V_{S_0}(b)$. □

Appendix B: Some calculation details

Here we provide the calculation details for the coefficients for cubic equilibrium equations (3.1). Assuming $i > 0$, equations from the model give us

$$C\beta s + \phi z - (\gamma + \mu) = 0,$$

which is

$$C\beta\left(1 - i - \frac{\gamma i}{\phi i + \mu}\right) + \phi\frac{\gamma i}{\phi i + \mu} - (\gamma + \mu) = 0$$

Multiplying by $\phi i + \mu$ this is

$$C\beta\Big((\phi i + \mu)(1 - i) - \gamma i\Big) - \mu(\mu + \gamma + \phi i) = 0.$$

Using that

$$C = \frac{C^s C^i}{sC^s + iC^i + zC^z} = \frac{C^s C^i}{i(C^i - C^s) + z(C^z - C^s) + C^i}$$
$$= \frac{C^s C^i(\phi i + \mu)}{i(\phi i + \mu)(C^i - C^s) + \gamma i(C^z - C^s) + C^s}$$

We have

$$C^s C^i \beta\Big((\phi i + \mu)(1 - i) - \gamma i\Big)(\phi i + \mu) - \mu(\mu + \gamma + \phi i)\Big(i(\phi i + \mu)(C^i - C^s) + \gamma i(C^z - C^s) + C^s(\phi i + \mu)\Big)$$
$$= 0$$

If we divide both sides by $(\mu + \gamma)^3$ this expression equals:

$$\underbrace{C^s R_0\Big((R_\phi i + R_\mu)(1 - i) - (1 - R_\mu)i\Big)(R_\phi i + R_\mu)}_{1}$$
$$\underbrace{- R_\mu(1 + R_\phi i)\Big(i(R_\phi i + R_\mu)(C^i - C^s) + (1 - R_\mu)i(C^z - C^s) + C^s(R_\phi i + R_\mu)\Big)}_{2} = 0$$

We simplify this expression. Note that

$$(R_\phi i + R_\mu)(1 - i) - (1 - R_\mu)i = R_\phi i - i^2 R_\phi + R_\mu - iR_\mu - i + iR_\mu$$
$$= -R_\phi i^2 - i(1 - R_\phi) + R_\mu.$$

So the expression 1 becomes:

$$- C^s R_0\Big(R_\phi i^2 + i(1 - R_\phi) - R_\mu\Big)(R_\phi i + R_\mu)$$
$$= -C^s R_0\Big[R_\phi^2 i^3 + (R_\phi R_\mu + R_\phi(1 - R_\phi))i^2 + R_\mu(1 - R_\phi)i - R_\mu R_\phi i - R_\mu^2\Big]$$
$$= -\Big[R_\phi^2 C^s R_0 i^3 + (R_\phi R_\mu C^s R_0 + R_\phi(1 - R_\phi)C^s R_0)i^2 + R_\mu(1 - R_\phi)C^s R_0 i - R_\mu R_\phi C^s R_0 i - R_\mu^2 C^s R_0\Big]$$

Also,

$$i(R_\phi i + R_\mu)(C^i - C^s) + (1 - R_\mu)i(C^z - C^s) + C^s(R_\phi i + R_\mu)$$
$$= R_\phi(C^i - C^s)i^2 + R_\mu(C^i - C^s)i + (1 - R_\mu)(C^z - C^s)i + C^s R_\phi i + C^s R_\mu$$
$$= R_\phi(C^i - C^s)i^2 + \big[R_\mu(C^i - C^s) + (1 - R_\mu)(C^z - C^s) + C^s R_\phi\big]i + C^s R_\mu.(*)$$

Multiplying $(*)$ by $(1 + R_\phi i)$ yields:

$$R_\phi(C^i - C^s)i^2 + \big[R_\mu(C^i - C^s) + (1 - R_\mu)(C^z - C^s) + C^s R_\phi\big]i + C^s R_\mu$$
$$+ R_\phi^2(C^i - C^s)i^3 + \big[R_\mu R_\phi(C^i - C^s) + (1 - R_\mu)R_\phi(C^z - C^s) + C^s R_\phi^2\big]i^2 + C^s R_\mu R_\phi i$$

Multiplying by R_μ gives us the full expression for 2 as:

$$R_\phi R_\mu(C^i - C^s)i^2 + \big[R_\mu^2(C^i - C^s) + R_\mu(1 - R_\mu)(C^z - C^s) + C^s R_\phi R_\mu\big]i + C^s R_\mu^2$$
$$+ R_\phi^2 R_\mu(C^i - C^s)i^3 + \big[R_\mu^2 R_\phi(C^i - C^s) + (1 - R_\mu)R_\phi R_\mu(C^z - C^s) + C^s R_\phi^2 R_\mu\big]i^2 + C^s R_\mu^2 R_\phi i$$

Removing the negative signs in front of each expression we get the next expression to equal zero.

$$R_\phi^2 C^s R_0 i^3 + (R_\phi R_\mu C^s R_0 + R_\phi(1 - R_\phi)C^s R_0)i^2 + R_\mu(1 - R_\phi)C^s R_0 i - R_\mu R_\phi C^s R_0 i - R_\mu^2 C^s R_0$$
$$+ R_\phi R_\mu(C^i - C^s)i^2 + \big[R_\mu^2(C^i - C^s) + R_\mu(1 - R_\mu)(C^z - C^s) + C^s R_\phi R_\mu\big]i + C^s R_\mu^2$$
$$+ R_\phi^2 R_\mu(C^i - C^s)i^3 + \big[R_\mu^2 R_\phi(C^i - C^s) + (1 - R_\mu)R_\phi R_\mu(C^z - C^s) + C^s R_\phi^2 R_\mu\big]i^2 + C^s R_\mu^2 R_\phi i$$

The free coefficient is

$$a_0 = C^s R_\mu^2(1 - R_0).$$

The principal coefficient, that is the i^3 coefficient, is

$$\begin{aligned} a_3 &= C^s R_\phi^2 R_0 + R_\phi^2 R_\mu(C^i - C^s) \\ &= R_\phi^2\big(C^s R_0 + \underbrace{R_\mu(C^i - C^s)}_{\textbf{extra}}\big). \end{aligned}$$

The coefficient with i^2 is

$$R_\phi R_\mu C^s R_0 + R_\phi(1 - R_\phi)C^s R_0 + R_\phi R_\mu(C^i - C^s) + R_\mu^2 R_\phi(C^i - C^s) + (1 - R_\mu)R_\phi R_\mu(C^z - C^s) + C^s R_\phi^2 R_\mu$$
$$= R_\phi\Big[R_\mu C^s R_0 + (1 - R_\phi)C^s R_0 + R_\mu(C^i - C^s) + R_\mu^2(C^i - C^s) + (1 - R_\mu)R_\mu(C^z - C^s) + C^s R_\phi R_\mu\Big]$$
$$= R_\phi\Big[C^s R_0(1 - R_\phi) + R_\mu(C^s R_0 + C^s R_\phi) + R_\mu(1 + R_\mu)(C^i - C^s) + (1 - R_\mu)R_\mu(C^z - C^s)\Big]$$

Rearranging a little bit,

$$a_2 = R_\phi\Big[C^s\left[R_0(1 - R_\phi) + R_\mu(R_0 + R_\phi) + R_\mu(1 - R_\mu)\left(\frac{C^z}{C^s} - 1\right)\right] + \underbrace{R_\mu(1 + R_\mu)(C^i - C^s)}_{\textbf{extra}}\Big].$$

Finally, the term with i equals

$$= R_\mu(1-R_\phi)C^sR_0 - R_\mu R_\phi C^s R_0 + R_\mu^2(C^i - C^s) + R_\mu(1-R_\mu)(C^z - C^s) + C^s R_\phi R_\mu + C^s R_\mu^2 R_\phi$$

$$= R_\mu\Big[(1-R_\phi)C^sR_0 - R_\phi C^s R_0 + R_\mu(C^i - C^s) + (1-R_\mu)(C^z - C^s) + C^s R_\phi + C^s R_\mu R_\phi\Big]$$

$$= R_\mu\Big[C^sR_0(1-R_\phi) + C^sR_\phi(1-R_0) + (1-R_\mu)(C^z - C^s) + C^s R_\mu R_\phi + \underbrace{R_\mu(C^i - C^s)}_{\textbf{extra}}\Big]$$

$$= R_\mu\Big[C^s\Big\{R_0(1-R_\phi) + R_\phi(1-R_0) + (1-R_\mu)\left(\frac{C^z}{C^s} - 1\right) + R_\mu R_\phi\Big\} + \underbrace{R_\mu(C^i - C^s)}_{\textbf{extra}}\Big]$$

Taking C^s as a factor out of all the coefficients we finally have that $+i$ satisfies a cubic equation $f(i) = a_3 i^3 + a_2 i^2 + a_1 i + a_0 = 0$, where the coefficients are given by

$$a_3 = R_\phi^2 R_0 + R_\mu R_\phi^2\left(\frac{C^i}{C^s} - 1\right)$$

$$a_2 = R_\phi\Big[R_0(1-R_\phi) + R_\mu(R_0 + R_\phi) + R_\mu(1-R_\mu)\left(\frac{C^z}{C^s} - 1\right) + R_\mu(1+R_\mu)\left(\frac{C^i}{C^s} - 1\right)\Big]$$

$$a_1 = R_\mu\Big[R_0(1-R_\phi) + R_\phi(1-R_0) + (1-R_\mu)\left(\frac{C^z}{C^s} - 1\right) + R_\mu R_\phi + R_\mu\left(\frac{C^i}{C^s} - 1\right)\Big]$$

$$a_0 = R_\mu^2(1-R_0).$$

CHAPTER 2

Adaptive behavior in Epidemiological Models

In this section we develop a theoretical frame for the adaptive contact decision algorithm and explore some of it's analytical properties. To understand the adaptive model's theoretical foundations we recall the Markov Decision Processes Theory and explain how it's application to epidemic models yields the adaptive algorithms. Alongside this, we perform numerical examples showing the adaptive response change and illustrate the challenges in studying the adaptive algorithm from the classical perspective. We conclude the chapter with an application of the adaptive decision process to network models. This last application exploits the connection between economical and epidemiological considerations individuals make when engaging in contacts in a network model.

Our purpose now will be to study the analytical behavior of the nonlinear relapse model proposed in the previous section, employing the adaptive setting methodology to compute and update the contact rates C^h for $h \in \{s, i, \widetilde{s}\}$ through time. This chapter is divided as follows: in section 6 we recall the theory of Markov Decision Processes, which is needed to understand the adaptive formulation. In section 7 we explain in detail the algorithm for the adaptive computation of contact rates using the theory discussed in the previous section. In section 8 we provide several numerical examples and experiments using the adaptive algorithm. In section 9 we prove some theoretical results regarding the adaptive algorithm. In section 10 we give an application of the adaptive setting to epidemiological network models.

6. Basic Theory of Markov Decision Processes

A Markov Decision Process is an abstraction used to model a process of decision making by an individual or agent. This concept is developed as a part of the discipline of Reinforcement Learning and is useful in many applications of Machine Learning to economics and robotics. We take the main definitions from [22, 30].

Definition 6.1. A (finite horizon [4]) Markov Decision Process $\mathcal{M}$ (from now on called MDP) consists of the following:

- A space of **states** $\mathcal{S}$.
- A space of possible **actions** $\mathcal{A}$.
- A **progression over a time axis** t. Where, for each t there's a state S_t and the need to make a decision to take an action A_t in order to move to the next time stage.

[4]There are infinite decision Markov Processes, however those will not be of our interest.

- An **immediate reward** $u^h : \mathcal{A} \to \mathbb{R}$ for each state h. Gives the reward/utility of choosing action a if the current state is h.
- For each time stage t and for each states $h, h' \in \mathcal{S}$, there's a **probability of transition** $p^t_{hh'} : \mathcal{A} \to [0,1]$, where $p^t_{hh'}(a)$ denotes *the probability that at time $t+1$ the state of the system becomes h' if at the current time the state is h and the agent takes decision a to move forward.* The matrix $P^t = (p_{hh'})_{hh'} \in \mathbb{R}^{|\mathcal{S}|\times|\mathcal{S}|}$ is called the **transition probability matrix** at time t.
- A **planning horizon** τ, decisions are made for $t = 1, \cdots, \tau$.

These are the settings under which a MDP takes place. We will denote an MDP as $\mathcal{M} = (\mathcal{S}, \mathcal{A}, p^t_{hh'}, u^t_h)$. Because these are the basic defining elements of the process. The actual decision that the agent makes at each time is what is known as a **policy**. First, for a finite space Ω, denote $\Delta(\Omega) := \{f : \Omega \to [0,1] \mid \sum_{\omega\in\Omega} f(\omega) = 1.\}$, the set of probability distributions over Ω.

Definition 6.2. Let $\mathcal{M} = (\mathcal{S}, \mathcal{A}, p^t_{hh'}, u^t_h)$ a MDP. A **policy** is a series of functions $\pi := \{\pi_t : \mathcal{S} \to \Delta(\mathcal{A}) \mid t = 1, \cdots, \tau\}$, which for every time t give the agent a probability density on the action space, depending on the state of the system. If for all t the decision rule π^t has a $a^t \in \mathcal{A}$ such that $\pi^t(a^t) = 1$ and $\pi^t(a) = 0$ for all $a \neq a^t$, then we say the policy is a **deterministic policy**.

There are many possibilities for policies to undertake, and at each step, the policy gives a probability distribution on how to choose the action to take, so the progress of the system is determined by the policy selection. How should the agent select an optimal policy? For this we formulate the basic **optimality criteria** of MDP's.

Definition 6.3 (Value function of a policy)**.** Let X_t, Y_t the random variables that denote the state and action at time $t = 0, 1, 2, \cdots, \tau$, respectively. Given a policy π and a distribution on the starting state $\beta \in \Delta(\mathcal{S})$, we can define the probability $P_{\beta,\pi}(X_t = s, Y_t = a)$, which is the probability that at time t the state is s and the action taken is a.

If the probability that the system starts at state h we write $P_{h,\pi}$. Now we define the value vector for π as $V^\pi \in \mathbb{R}^{|\mathcal{S}|}$, with h-th entry -for h in $\mathcal{S}$- given by:

$$V^\pi(h) = \sum_{t=1}^{\tau} \delta^{t-1} \sum_{h',a} P_{h,\pi}(X_t = h', Y_t = a).$$

Where $\delta \in [0,1]$ is a **discount factor**. A policy π^* is an **optimal** policy, if for all $h \in \mathcal{S}$ and all other policies we have $V^{\pi^*}(h) \geq V^\pi(h)$.

The literature of MDP's describes a procedure to find an optimal policy. This was first described by Richard Bellman in 1957.

Definition 6.4. The optimal deterministic policy π^* for a finite horizon MDP is obtained through a process of *backwards induction*. For each state $h \in \mathcal{S}$, we define the value function $V_t(h)$ at time t. The optimal $a \in \mathcal{A}$ to choose at time t when state is h (this is $\pi^*_t(h)$) is computed using the

Bellman Equation for $V_t(h)$, given by

$$V_t(h) = \max_{a \in \mathcal{A}} \left\{ u^h(a) + \delta \sum_{h' \in \mathcal{S}} p^t_{hh'}(a) V_{t+1}(h') \right\}, \tag{6.1}$$

where δ is the discount factor. The process of backwards induction starts with an initial vector ($V_{t+\tau+1}(h)$ for each $h \in \mathcal{S}$) and moves backwards in time using Bellman's equation to find $V_t(h)$. At each time t the argmax of $V_t(h)$ is the action to select (that is, the value of $\pi^*_t(h)$).

7. Formulation of Adaptive Behavior Model

The adaptive setting provides an algorithm to compute and update the contact rates C^h in the model discussed last section. We recall our differential equation model is

$$\begin{aligned} \frac{dS}{dt} &= -g(\cdot)\beta \frac{SI}{N} + \mu N - \mu S, \\ \frac{dI}{dt} &= g(\cdot)\beta \frac{SI}{N} + \phi \frac{\widetilde{S}I}{N} - (\gamma + \mu) I, \\ \frac{d\widetilde{S}}{dt} &= \gamma I - \phi \frac{I\widetilde{S}}{N} - \mu \widetilde{S}. \end{aligned} \tag{7.1}$$

where

$$g(S, I, \widetilde{S}) = \frac{C^s C^i N}{SC^s + IC^i + \widetilde{S}C^{\widetilde{s}}}, \tag{7.2}$$

is our incidence function. Here, each contact rate is of the form $C^h = C^h(S(t), I(t), \widetilde{S}(t))$, that is, they are not constant and they depend on the states of the system at each time. These functions are updated in steps of length $\Delta t = 1$, representing the daily update made in individuals decision. The process involves the creation of an MDP for each daily time-step. We describe this process in detail.

Adaptive Computation Process

For time t_0, we have the current values of our system $(S(t_0), I(t_0), \widetilde{S}(t_0))$, we use them to project the system over a time frame of τ days, that is, over the time period $[t_0, t_0 + \tau]$. We call this projection $(S^{t_0}, I^{t_0}, \widetilde{S}^{t_0})$. This is a hypothetical projection performed by the decision agent to assess the near future of the disease. We consider a MDP $\mathcal{M}_{t_0}$ of finite horizon τ, consisting of the following:

- The state state $\mathcal{S} = \{s, i, \widetilde{s}\}$, the possible states for an individual at the epidemic system.
- The action state $\mathcal{A} = [0, C_{\max}]$, an interval of possible contact rates that can be made by an individual per time period.
- The immediate rewards $u^h_t(a)$, concave functions with a global maximum.

- The transition probability matrix, for each $t = t_0, \cdots, t_0 + \tau$, in this case is given by

$$\begin{pmatrix} p^t_{ss}(a) & p^t_{si}(a) & p^t_{s\widetilde{s}}(a) \\ p^t_{is}(a) & p^t_{ii}(a) & p^t_{i\widetilde{s}}(a) \\ p^t_{\widetilde{s}s}(a) & p^t_{\widetilde{s}i}(a) & p^t_{\widetilde{s}\widetilde{s}}(a) \end{pmatrix} = \begin{pmatrix} 1 - p^t_{si}(a) & p^t_{si}(a) & 0 \\ 0 & 1 - p^t_{i\widetilde{s}}(a) & p^t_{i\widetilde{s}}(a) \\ 0 & p^t_{\widetilde{s}i}(a) & 1 - p^t_{\widetilde{s}i}(a) \end{pmatrix}.$$

The entries are defined as

$$p^t_{si}(a) = 1 - \exp\left(-\beta a \frac{I^{t_0}(t) C^{i*}_{t_0,0}}{S^{t_0}(t) C^{s*}_{t_0,0} + I^{t_0}(t) C^{i*}_{t_0,0} + \widetilde{S}^{t_0}(t) C^{\widetilde{s}*}_{t_0,0}} \right), \tag{7.3}$$

$$p^t_{i\widetilde{s}}(a) = 1 - e^{-\gamma}, \tag{7.4}$$

$$p^t_{\widetilde{s}i}(a) = \lambda p^t_{si}(a). \tag{7.5}$$

These are, respectively, the probability of infection for susceptibles, the probability of recovery and the probability of reinfection. Here $\lambda \geq 0$ is a multiplier connecting the probability of infection before and after being afflicted with the disease. Only when the model doesn't present relapse phenomena (that is when $\phi = 0$) we use $\lambda = 0$. The values $C^{h*}_{t_0,0}$ are set as constants initially in this process, and correspond to estimations on the general behavior of all other individuals in this time frame.

For the computation of the optimal policy we have value function vectors

$$V_t = \begin{pmatrix} V_t(s) \\ V_t(i) \\ V_t(\widetilde{s}) \end{pmatrix}, \qquad \text{for each } t = t_0, t_0 + 1, \cdots, t_0 + \tau + 1.$$

Each value function is computed using Bellman's equation. There is one for each health status, and they are given by

$$V_t(s) = \max_{a \in \mathcal{A}} \left\{ u^s(a) + \delta \left[(1 - p^t_{si}(a)) V_{t+1}(s) + p^t_{si}(a) V_{t+1}(i) \right] \right\}, \tag{7.6}$$

$$V_t(i) = \max_{a \in \mathcal{A}} \left\{ u^i(a) + \delta \left[(1 - p^t_{i\widetilde{s}}(a)) V_{t+1}(i) + p^t_{i\widetilde{s}}(a) V_{t+1}(\widetilde{s}) \right] \right\}, \tag{7.7}$$

$$V_t(\widetilde{s}) = \max_{a \in \mathcal{A}} \left\{ u^{\widetilde{s}}(a) + \delta \left[\lambda p^t_{si}(a) V_{t+1}(i) + (1 - \lambda p^t_{si}(a)) V_{t+1}(\widetilde{s}) \right] \right\}. \tag{7.8}$$

Using these equations and the procedure of backwards induction we find the optimal policy π^*_t. The optimal values to select from this MDP are $C^{h*}_{t_0} = \pi^*_{t_0}(h)$ for each $h \in \{s, i, \widetilde{s}\}$. That is the values of the policy at the start of the process. This is intuitive, as the MDP is a projection the individual performs in their minds, getting the value of the projection at the start would constitute what they should today according to said projection. This gives the optimal selection at time period t_0. [5]

[5]The process is done with constant values $C^{h*}_{t_0,0}$ that represent the general decision of all other individuals of this health status. After the backwards induction optimization we end up with a value $C^{h*}_{t_0}$, which is choice of the decision agent under consideration. This distinction is highlighted in [15].

Having this selection of contact rates, we solve the system (7.1) from t_0 to $t_0 + 1$ using the optimal values $C_{t_0}^{h*}$ found from the MDP $\mathcal{M}_{t_0}$. Then, we move to time t_0+1, we have another state $(S(t_0 + 1), I(t_0 + 1), \widetilde{S}(t_0 + 1))$, here we make another MDP $\mathcal{M}_{t_0+1}$ and continue in this fashion, taking jump times of $\Delta t = 1$ days. The following figure illustrates this algorithm.

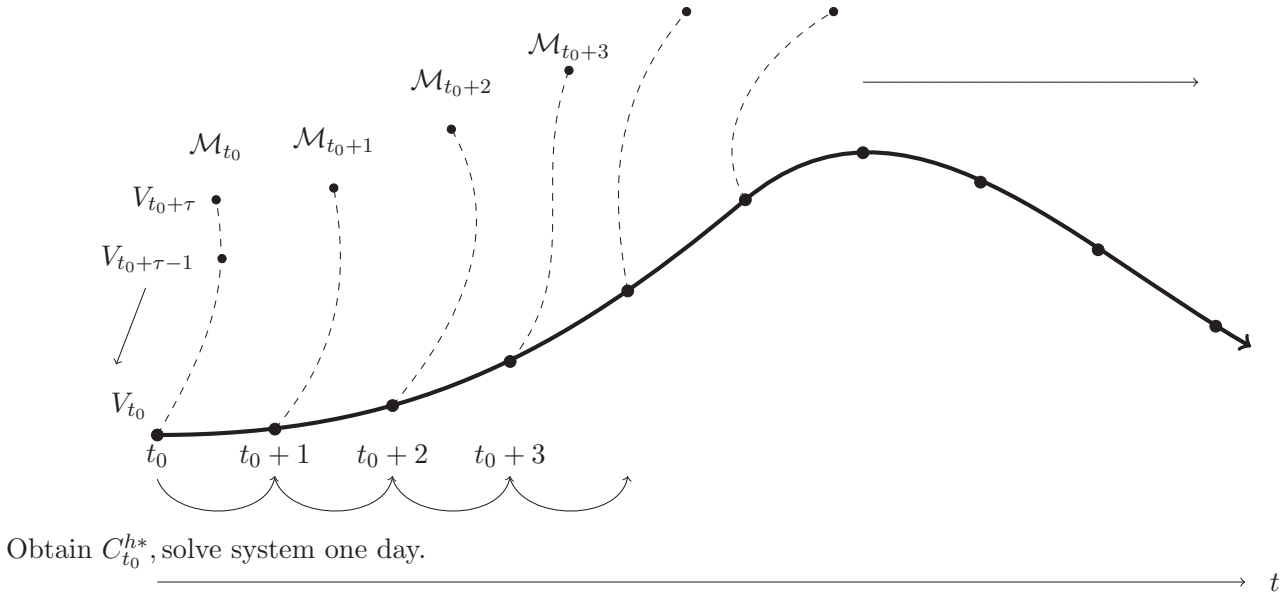

FIGURE 9. Illustration of the adaptive setting, at each discrete time t_0 a hypothetical projection over a horizon τ is computed in order to update the contact rates values using a MDP $\mathcal{M}_{t_0}$.

Therefore, the adaptive algorithm involves solving a series of MDP's and updating the system's values day by day.

Remark 7.1. As we can see, the adaptive algorithm involves the application of the theory of MDPs, however it requires solving one MDP per discrete time step. We therefore have a series of decision processes $\{\mathcal{M}_t\}_{t=0}^{\infty}$. These decision processes are connected with each other by solving the differential equation system. The idea behind this chain of decision processes is to update the behavior of the individual every day, taking into consideration the current state of the disease and a projection on its near future. When there is no reinfection ($\phi = \lambda = 0$), values of $V_t(i)$ and $V_t(z)$ are constant, thus making C_t^{i*} and $C_t^{\widetilde{s}*}$ also constant and achieved at the values that maximize u_i and $u_{\widetilde{s}}$ respectively.

Remark 7.2. Given that $(1 - p_{i\widetilde{s}}^t(a))V_{t+1}(i) + p_{i\widetilde{s}}^t(a)V_{t+1}(\widetilde{s})$ is a constant that doesn't depend on a for each t, the selected a^{i*} at each time t will equal the optimal of $u^i(a)$, making the behavior of infected individuals to be non-adaptive.

8. Numerical Examples and Experiments

In this section we illustrate the results this algorithm has on the epidemic behavior, highlighting differences between this setting and the classical formulation. We also provide some sensitivity analysis of the adaptive algorithm towards the model parameters and we construct some conjectures on the general behavior of adaptive models.

Our implementation of the adaptive algorithm is based in `python` and it is available in [6]. The `code/adaptive/MDP` module implements the basic backwards induction procedure for a general MDP, this is used in the `code/adaptive/adaptive_MDP` module, in which the optimal C^{h*} are computed at each discrete time t by performing a MDP optimal policy inspection. The notebook `code/adaptive/adaptive_use` offers an example on how to use this module (mainly the examples discussed in this section). The path `code/disaggregated` contains code for the model proposed in the first chapter.

To start, let's see some numerical examples where we apply this method and compare to previous classical settings.

Example 8.1 (An example without relapse)**.** First, we look at the base example given in the original source, [15]. Here our model parameters are $\beta = 0.0925, \quad \mu = 0, \quad \phi = 0, \quad \gamma = 0.1823$. The utility functions are in this case given by the semi-quadratic expressions

$$u_h(a) = (b_h \cdot a - a^2)^\nu - a_h \tag{8.1}$$

for $h \in \mathcal{S} = \{s, i, \widetilde{s}\}$. These functions are concave and attain a single global maximum at $a = b_h/2$. The global maximum of u_h will be denoted by C^{h*}_{opt}. These functions represent the immediate reward of engaging in contacts for an individual in health class h. Using semi-quadratic utility functions like these is intuitive: we expect that the utility increases as contacts increase, but there is a moment where having too many contacts can be dangerous (possibly due to reasons related to the transmission of the disease through contacts with others) so the utility starts to decrease from that point forward.

In this example we use $b_s = b_{\widetilde{s}} = 10, \quad b_i = 6.67, \quad a_s = a_{\widetilde{s}} = 0, \quad a_i = 1.826, \quad \nu = 0.25$. Our discount factor is $\delta = 0.99986$ and, finally, our horizon is given by $\tau = 12$. We start with a null infected population. The next figure shows a very important comparison.

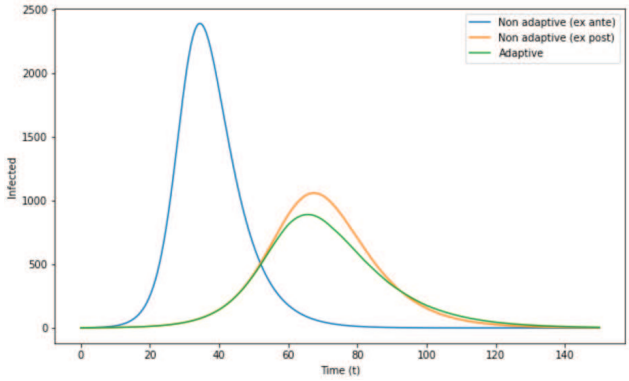

FIGURE 10. Comparison of infected populations between classical model (ex-ante), disaggregated model (ex-post) and full adaptive model. Same as Figure 1A in [15].

Here we present the infected population behavior under three models: the adaptive model, the non-adaptive ex-ante model in which we use $C^h = b_s/2$ for all $t \geq 0$ and the non-adaptive ex-post model where we use $C^h = b_h/2$ (the optimal of the utility function u_h) for all $t \geq 0$. The ex-ante model represents the classical model, in which all health populations behave in a homogeneous manner. The ex-post model introduces heterogeneity into health classes but doesn't allow individuals to adapt their behavior (this is the spirit of the model we proposed in the first chapter). The adaptive model allows for contact rate modification throughout the disease progress. The next figure shows the adaptive behavior in action, as we can see how susceptible individuals have altered their contact rates according to the progress of the disease.

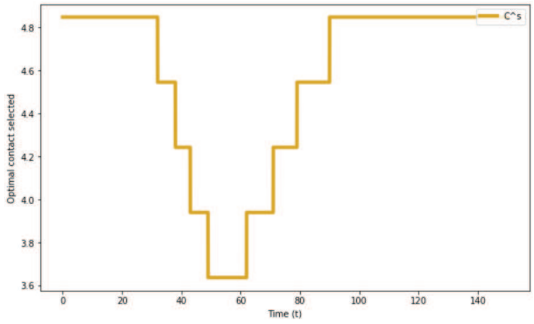

FIGURE 11. Plot of optimal C^{s*} achieved at each time step

This example shows that the classical model assumptions can often over-estimate the true behavior of the disease, because it doesn't take into account the utility and risk considerations agents make in the progress of the epidemic. The reader can verify that, when using $\phi = \lambda = 0$, then the values of $V_t(i)$ and $V_t(\widetilde{s})$ remain constant at each $\mathcal{M}_t$, which implies C^i and $C^{\widetilde{s}}$ are also constant, and the only contact rate to undergo adaptive behavior is C^s. This is the original conception from [15], and is inspired in the fact that, without reinfection, infected and recovered individuals don't experience any gain or loss in altering their contacts through time.

Example 8.2 (Effect of τ)**.** The planning horizon has an important effect on the adaptive behavior results, as said by [15]: *Intuitively, a larger τ increases $V_{t+1}(s)$, as there is more time to gain benefits either by staying healthy or from having more time to recover.* The next figure shows the minimal C^{s*} achieved by susceptible individuals varying the planning horizon τ, we use the parameters from the previous example. This result is, however, dependant on the utility functions used. For example, if we remove the constant term a_i and make $a_i = 0$, we observe the effect that τ has on the system.

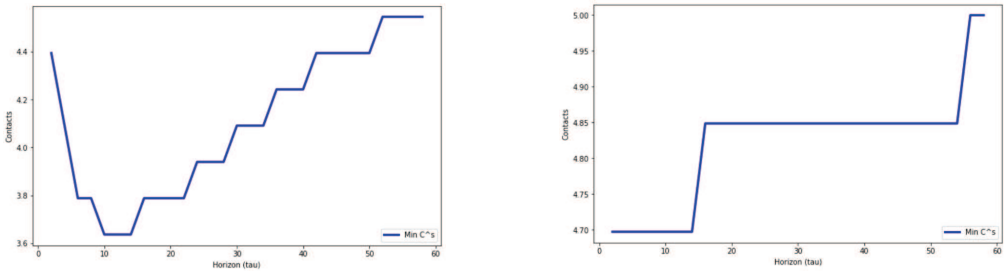

FIGURE 12. A small increase in τ makes $V_{t+1}(s)$ to increase faster than $V_{t+1}(i)$, however increasing τ reduces this effect and the minimal C^{s*} increases again. On the right, a different behavior increasing τ when $a_i = 0$

Example 8.3 (Effect of β)**.** In the last example we saw a change by tweaking the utility functions. We need to take into account the form of Bellman's optimality equation for this. Note that the derivation of value functions is dependant on both the utility functions and on the values of the transition probabilities. Changing one or the other could lead to very different results.

For example, let's continue with the original parameters from example 8.1, but this time we reduce the value of β to $\beta = 0.0725$ (a reduction of a 22%). If we solve the system with the adaptive algorithm we get the following C^{s*} history.

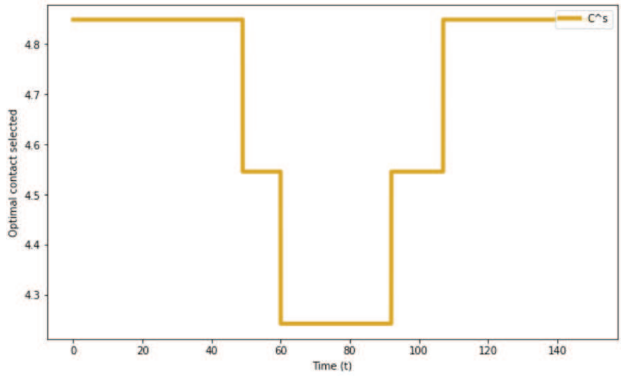

FIGURE 13. Plot of optimal C^s achieved at each time step, using $\beta = 0.0725$.

Comparing with figure 11, we see a smaller variation on optimal contact rates. We can deduce this from Bellman's equation. Reducing β will in turn reduce p_{si} which will make the second part of the optimality equation to weigh less with respect to $u_s(a)$, this will make the final decision closer

to the optimal of the utility function u_s. Here we can see the effect of β on the adaptive variability of C^{s*}.

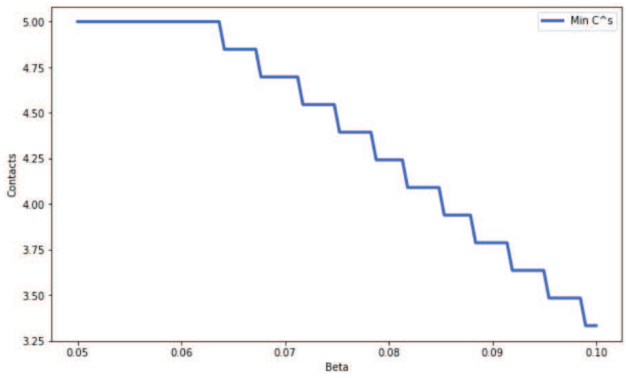

FIGURE 14. Reducing β makes the adaptive algorithm to fade away and brings the possible final contact decision closer to the optimal of u_s (which is $a = 5$ in this example).

Naturally, increasing β makes it more likely to become infected thus increasing the disease infection peak. We conclude that adaptive considerations become more influential as the disease infection rate increases. Here the optimal of the utility function is $C^{s*}_{\text{opt}} = 5$.

Example 8.4 (An example with non-linear relapse)**.** Here we apply the adaptive model in the case of non-linear relapse and annotate the changes with respect to the previous examples. If we use the parameters from the example in the last chapter:

$$\beta = 0.00096, \quad \mu = 0.00015, \quad \phi = 0.044, \quad \gamma = 0.0027,$$

along with utility functions of the form in 8.1 with $b_s = 24$, $b_i = 20$ and $b_{\widetilde{s}} = 30$ (making, thus, the respective optimal utility contacts to be $C_0^{s*} = 12, C_0^{i*} = 10$ and $C_0^{\widetilde{s},*} = 15$). In this case we also get an adaptive response for the contact rates of the $\widetilde{S}$ population.

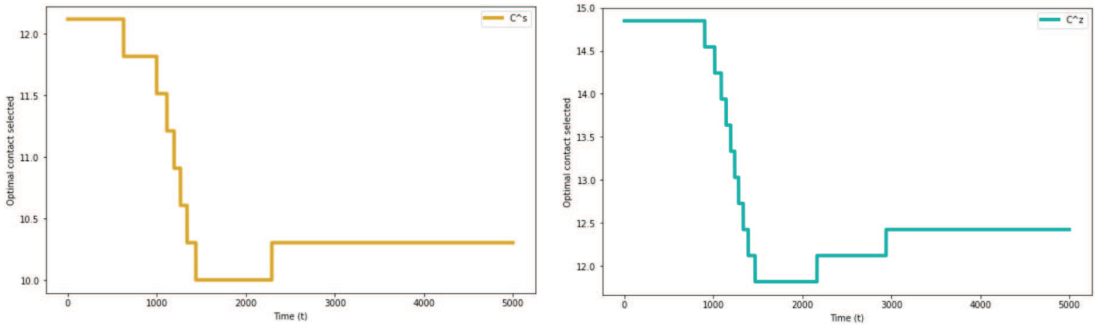

FIGURE 15. For a model with relapse, we have adaptive considerations in both susceptible and temporarily recovered individuals.

For this example we see on the left the history of selected optimal C^s contact rates; on the right the history for C^z. We compare this with the disaggregated model we discussed in the previous

chapter. The *ex-ante* model in this case represents the model with no adaptive behavior, in which individuals just select the optimal contact rate for their utility functions $C^{h*} = C_0^{*h}$ for all $h \in \mathcal{S}$. Naturally, in the adaptive setting, this rate is modified (as we saw in the previous figure) so we could compare the adaptive model to the *ex-post* model, in which we model the disease using the final contact rates obtained in the adaptive setting. We could think of the adaptive model as being **in between** these two models. Here we see the infected population comparison.

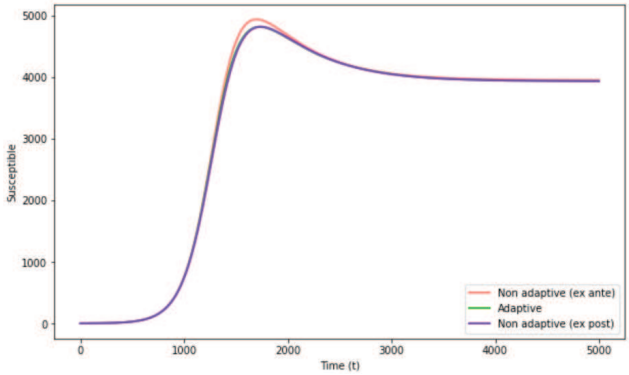

FIGURE 16. Comparison between the ex-ante, ex-post and adaptive models in this relapse example.

The difference might not be that noticeable because of the scale. To get a better picture the following plot presents the differences between infected populations in the three models.

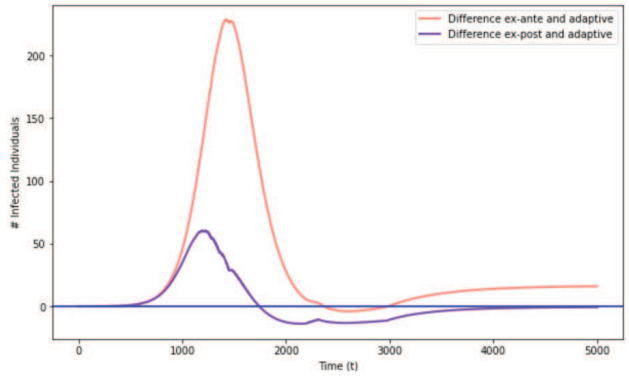

FIGURE 17. Plot of the differences $\Delta_1 = I_{\text{ex-ante}} - I_{\text{adaptive}}$ (in red) and $\Delta_2 = I_{\text{ex-post}} - I_{\text{adaptive}}$ (in purple), for each time t.

We can see that the ex-post model ends up being closer to the adaptive model and they both seem to converge to the same final infected equilibrium. They both produce a smaller infected steady state that the ex-ante model.

Remark 8.5. Although both algorithms offer different responses in the most critical periods of the disease, in this example the adaptive algorithm behaves very similarly to the ex-post algorithm in the stable stages of the disease. This leads us to conjecture that this behaviour holds in general

and it explains the relationship between the adaptive model with relapse in this section, and the ex-post model that uses the disaggregated approach in the previous chapter. This result would essentially say that the adaptive behavior cancels out at the stable final region and the model will behave as it was performed with constant asymptotic contact rates from the beginning.

This attests to the adaptive algorithm's importance during the most critical times of the epidemic but also shows that the adaptive considerations become irrelevant in more stable periods, and that at those moments, agents behave as if they had never indulged in adaptive computations before. This attests to a certain *markovian* property of the algorithm.

This situation occurs in several numerical examples performed ad-hoc during our research, however large-scale simulations were not performed during this research due to time constraints. Also, attempting to prove a result like this represents an important analytical challenge falling out of the scope of this project.

Example 8.6 (Effect of utility function shape)**.** As we have seen, the adaptive algorithm performs a selection of contact rates at each time step, which acts as a deviation from the utility function optimal point, C^{h*}_{opt}. Nonetheless, we perform the adaptive algorithm with two sets of utility functions, each having the same optimal value, but with different shapes. We use the parameters from example 8.1 (no relapse). The next plot shows two different utility functions for u_s, both having an optimal contact number of $C^{s*}_{\text{opt}} = 5$.

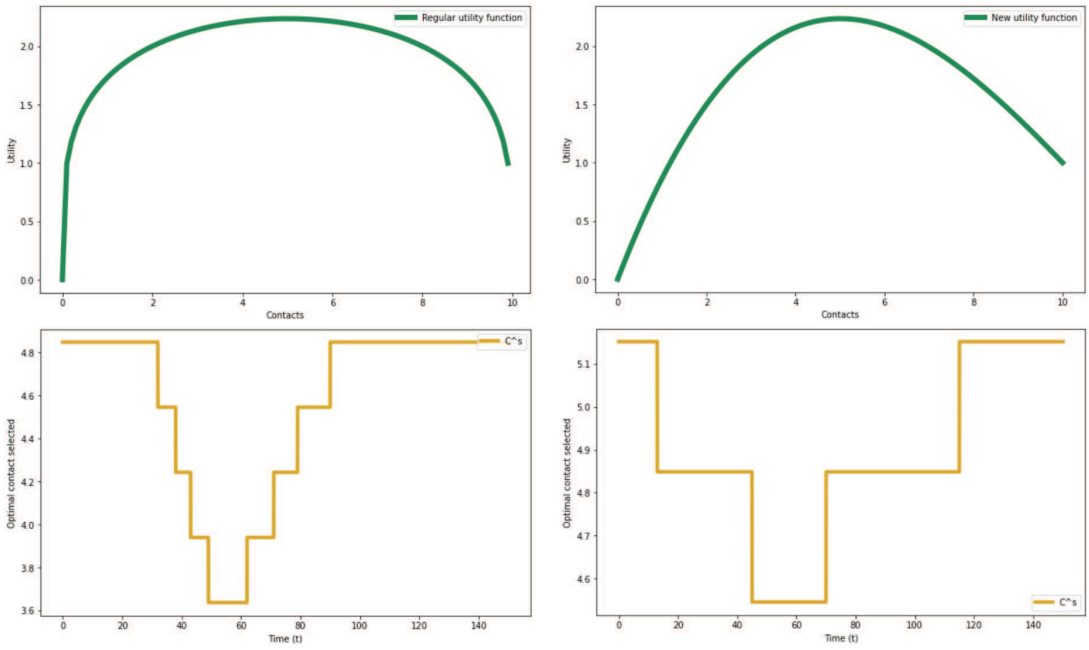

FIGURE 18. Adaptive responses for different shapes of utility functions.

On the top row, on the left a utility function $u^s(a) = (b_s \cdot a - a^2)^\nu$, on the right a polynomial utility function that has the same optimal point as the former. The bottom row shows the history of C^{s*}_t for each corresponding utility function.

We see a difference in the severity of the adaptive behavior. The higher slope on the utility function on the left makes the immediate reward considerations weigh more on the agent's decision, making the final contact to deviate less from the optimal point. Naturally, this implies that utility shape also affects the peak prevalence of the epidemic, because of the smaller scale of the adaptive behavior.

In most of the previous example we have seen that the adaptive method acts as a perturbation on the individual's decision making. If no adaptive behavior was present, then each agent would only select it's optimal contact rate, which is the optimal point of their utility function, C^{h*}_{opt}. However the adaptive behavior will force agents to weight their utility with the current state of the disease and their own projections about it. In order to quantify the effect of the adaptive behavior we introduce this definition.

Definition 8.7. Let $\mathbf{M} = (S(t), I(t), \widetilde{S}(t))$ a solution to 7.1 computed with the adaptive algorithm. For each $h \in \mathcal{S}$ we define

$$\Delta(C^h) := \max_{t \geq 0} |C^{h*}_t - C^{h*}_{\text{opt}}|$$

as the maximum difference between any contact decision made by agent in state h and their optimal immediate reward contact decision, at the solution $\mathbf{M}$.

We make the following conjecture, based on the previous examples (example 8.3 and 8.6). Note that the nature of this result is very general and not quantifiable (meaning that we don't have an exact mathematical relationship between the affecting parameters and the outcome).

Conjecture 8.8. *In solving model 7.1 with the adaptive setting, the value of $\Delta(C^h)$ has a direct relationship with β and an inverse relationship with the curvature of the utility function u^h near the optimal point a^{h*}_{opt}.*

Remark 8.9. This relates to the sensitivity analysis performed in [15], where the effect is measured over the minimum contacts attained. Note that the minimum contacts C^{h*}_{min} have an inverse relationship with $\Delta(C^h)$ because $\Delta(C^h) = C^{h*}_{\text{opt}} - C^{h*}_{\text{min}}$, so the direct relationship between $\Delta(C^h)$ and β corresponds to an inverse relationship between C^{h*}_{min} and β. And, indeed, sensitivity analysis performed in [15] shows that an increase of 10% in β yields a decrease of 10.5% in C^{s*}_{min}.

Remark 8.10. The relationship between $\Delta(C^h)$ and the utility function curvature is stated in the sensitivity analysis performed in [15]. In the case of utility functions of the form 8.1, the value of ν relates to the utility function curvature. According to [15], an increase of 10% in ν results in an increase of 3.2% increase in minimum of contacts (thus decreasing $\Delta(C^h)$).

Remark 8.11. We can provide a motivation for conjecture 8.8 based on Bellman's equation. We recall that the conditions to find an optimal contact policy were obtained with the backwards

iteration process given by the recursive relation (for $h = s$):

$$V_t(s) = \max_{a \in \mathcal{A}} \left\{ u^s(a) + \underbrace{\delta \Big[(1 - p^t_{si}(a)) V_{t+1}(s) + p^t_{si}(a) V_{t+1}(i) \Big]}_{\rho^t(a)} \right\}.$$

Let us consider the function inside this maximum. We know the form of $p^t_{si}(a)$, which is given by $p^t_{si}(a) = 1 - \exp(-\beta \vartheta_t a)$, where ϑ_t is a constant determined by the projection of the system τ days ahead. This makes the function inside the max argument of $V_t(s)$ to be of the form

$$u^s(a) + \underbrace{\exp(-\beta \vartheta_t a) \cdot \delta \big(V_{t+1}(s) - V_{t+1}(i) \big) + \delta V_{t+1}(i)}_{\rho^t(a)}.$$

Assuming $V_{t+1}(s) - V_{t+1}(i) > 0$, we have that ρ^t is a decreasing function in a. The main idea of the adaptive algorithm is to alter the optimal point a^{h*}_{opt} of u^h by adding the function ρ^t at each time step. The next plot shows how this optimal point deviation works.

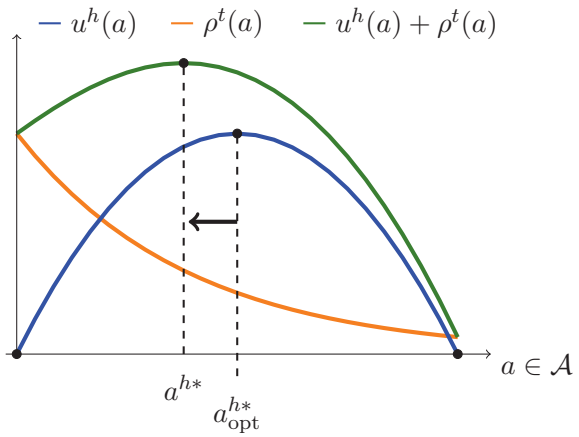

FIGURE 19. Illustration of how the optimality Bellman conditions shift the optimal contact point selected, away from the utility optimal.

As we can see, this explains why our simulations give us a decrease in the selected contacts for some time periods: the values of the state of the system make ρ^t strong enough to alter the optimal of u^h. Altering the sizes of the model parameters can modify this situation, for example, if the function ρ^t becomes less dominant then the deviation is smaller.

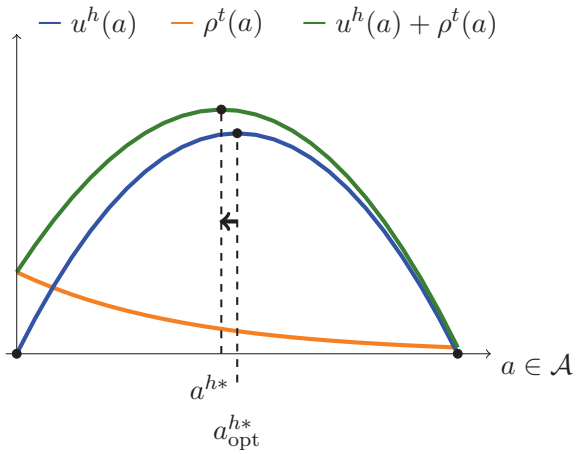

FIGURE 20. Illustration of how the optimality Bellman conditions shift the optimal contact point selected, away from the utility optimal. Reducing the importance of ρ^t.

If $\beta \to 0$ then $\rho^t(a)$ tends to be a constant function, making the deviation non significant. Also, if u^h has a bigger curvature, then the deviation also diminishes. See Figure 21 for an illustration.

A detailed proof of conjecture 8.8 can be found in the next section, and it uses this heuristic (see Theorem 9.2). Plots in Figure 21 will prove very useful in further applications of the adaptive algorithm in the next section.

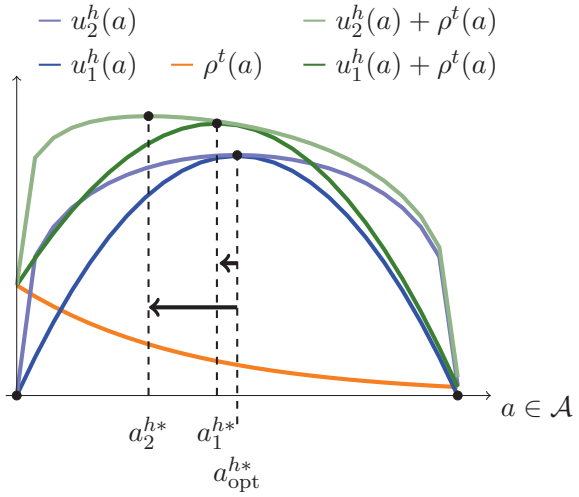

FIGURE 21. Illustration of how the optimality Bellman conditions shift the optimal contact point selected, away from the utility optimal.

Effect of utility function curvature: u^h_1 has a higher curvature than u^h_2, therefore it creates a smaller deviation from $a_{\text{opt}^{h*}}$ (compare a^{h*}_1 with a^{h*}_2).

Example 8.12 (Effect of differences across utility optimals.)**.** We could perform a bifurcation analysis similar to the one done in chapter 2, taking the proportions between contact rates of

different health statuses, however in this case the contact rates are not constant, and we have functions through time given by $\kappa(t) := \frac{C_t^{i*}}{C_t^{\tilde{s}*}}$ and $\theta(t) := \frac{C_t^{\tilde{s}*}}{C_t^{s*}}$. However, in this setting, these can change through time, and the initial values $\kappa(0), \theta(0)$ might be different at the final stages of the disease. Here we have a plot of $\theta(t)$ through time, using parameters in 8.4. We don't see any particular behavior or relationship during the adaptive period.

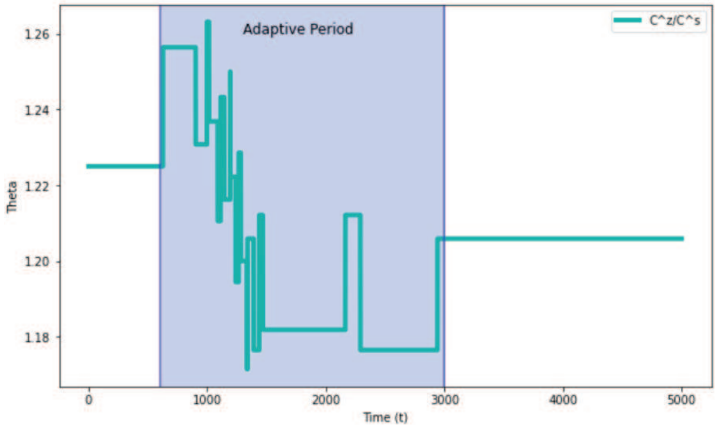

FIGURE 22. Plot of $\theta(t)$ using the adaptive model for parameters in example 8.4.

The initial value $\theta(0) \approx 1.225$ changes to a final $\theta_{\text{final}} \approx 1.2058$. This change is obtained after going through the adaptive period.

The following graph shows the relationship between the *apparent* R_0 and the final attained point $i^* = I^*/N$. Here, we define the apparent R_0 as $R_0^{\text{apparent}} := \frac{\beta C_{\text{opt}}^{i*}}{\gamma+\mu}$, which is the R_0 of the system without the adaptive effect. This plot shows convergence points for each R_0^{apparent} by varying the initial conditions, $x_0 = \big(N - \lfloor \rho N \rfloor, \lfloor \rho N \rfloor, 0\big)$ using a parameter $0 < \rho < 1$ [6].

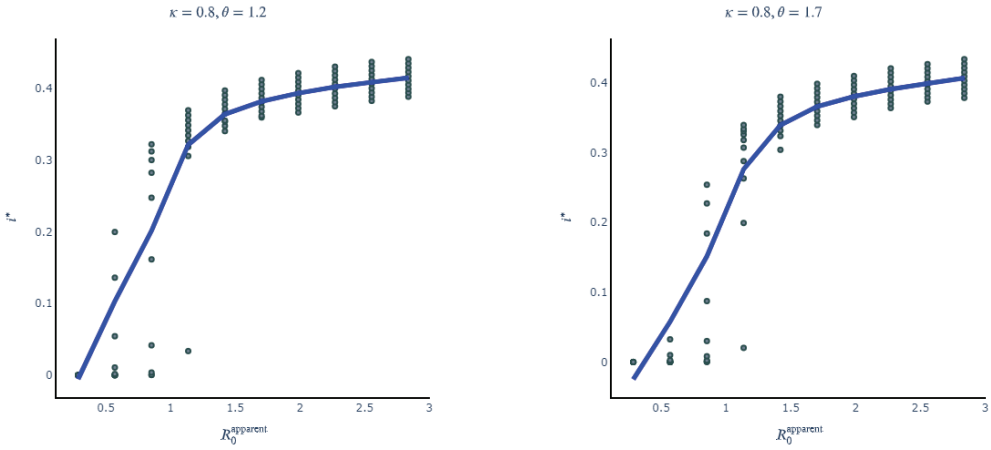

FIGURE 23. Different convergence points for each apparent R_0 using $\kappa(0) = 0.5$ and $\theta(0) = 1.2$, on the left and $\kappa(0) = 0.8, \theta(0) = 1.7$ on the right.

[6] As in the previous chapter, convergence points are obtained using a stopping point criteria of determining when subsequent daily solutions are sufficiently close to each other.

We see that in the adaptive setting there is more variance as to the final point obtained. The blue line represents the mean convergence point attached at each R_0 apparent.

In these plots, we see a very different behavior compared to the one in last chapter. Not only we have an absence of a clear backwards bifurcation, but we also have much smaller, pseudo-disease free states for high R_0's (> 1). This example can give us an idea of the difficulty of working with adaptive models, where, as we can see, the initial conditions are not as strong in determining the final behavior of the solution.

We do find a *critical* interval $[1, 1 + \epsilon(\kappa, \theta)]$ where there are diverse epidemiological scenarios possible, and more stable regions like $[\epsilon(\kappa, \theta), \infty)$. We hope the reader can comprehend from these examples, that the classical analysis falls somewhat short in the adaptive setting, and that there is the need for the development of new analytical techniques to tackle this problem.

9. Some Theoretical Results

We provide mathematical proofs for some of the statements done in the last section. We start with proving rigorously conjecture 8.8. Before that, we need the a simple lemma on continuous functions over compact sets.

Lemma 9.1. *Let $f : I \subseteq \mathbb{R} \to \mathbb{R}$ a continuous function defined over a compact subset $I \subseteq \mathbb{R}$ and $b \in f(I)$. Then for all $\epsilon > 0$, there exists $\delta > 0$ such that for all $a \in I$ with $|f(a) - b| < \delta$, then $d(a, f^{-1}(b)) < \epsilon$, where we define*

$$d(a, S) = \min_{t \in S} |a - t|,$$

for a closed subset $S \subseteq I$.

Proof. By contradiction we assume there is $\epsilon_0 > 0$ such that for all $\delta > 0$ there is $a_\delta \in I$ such that $|f(a_\delta) - b| < \delta$ and $d(a_\delta, f^{-1}(b)) \geq \epsilon_0$. Taking $\delta = \frac{1}{n}$ for $n \in \mathbb{N}$ we have a sequence $\{a_n\}_{n=1}^{\infty} \subseteq I$ such that $|f(a_n) - b| < \frac{1}{n}$ and $d(a_n, f^{-1}(b)) \geq \epsilon_0$ for all $n \in \mathbb{N}$. By the Bolzano-Weierstrass theorem, there is a convergent subsequence $\{a_{n_k}\}_{k=1}^{\infty}$ with $a_{n_k} \longrightarrow a_0 \in I$. Being f continuous, then $f(a_{n_k}) \to f(a_0)$, and the fact that $|f(a_n) - b| < \frac{1}{n}$ implies that $f(a_0) = b$, so $a_0 \in f^{-1}(b)$. Then, having $a_{n_k} \to a_0 \in f^{-1}(b)$ and $d(a_{n_k}, f^{-1}(b)) \geq \epsilon_0$ would be a contradiction, thus proving that the assertion in the lemma must be true. □

Theorem 9.2. *Let $h \in \{s, \widetilde{s}\}$, a non-infected health status. Assume $u^h \in \mathcal{C}^2(I)$ for some compact interval $I \subset \mathbb{R}_{>0}$, and that u^h attains a unique global maximum in I given by a^{h*}_{opt}. Suppose further that $(u^h)'' \neq 0$ in I. Then, except for keeping τ, δ and $\max_{h' \in \mathcal{S}} ||u^{h'}||_{\infty, I}$ constant, the following limits are achieved independently of the initial conditions or all the other parameters of the epidemiological model following the adaptive algorithm.*

$$(\boldsymbol{A}) \quad \lim_{\beta \longrightarrow 0} \Delta(C^h) = 0,$$

$$(\boldsymbol{B}) \lim_{||1/(u^h)''||_{\infty, I} \longrightarrow 0} \Delta(C^h) = 0.$$

Proof. We write the proof for $h = s$. The case $h = \widetilde{s}$ is analogous as the probability transition functions are multiples of p_{si}. Now, fix $t_0 > 0$ and consider the Markov Decision Process $\mathcal{M}_{t_0}$. For each $t \in \{t_0, t_0 + 1, \cdots, t_0 + \tau\}$, the optimization for $V_t(s)$ requires finding

$$V_t(s) = \max_{a \in \mathcal{A}} \left\{ u^s(a) + \rho^t(a) \right\},$$

where $\rho^t(a)$ is given by

$$\rho^t(a) = A_t e^{-\beta \vartheta_t a} + B_t,$$

where

$$\begin{aligned} \vartheta_t &= \frac{I^{t_0}(t) C^{i*}_{t_0,0}}{S^{t_0}(t) C^{s*}_{t_0,0} + I^{t_0}(t) C^{i*}_{t_0,0} + \widetilde{S}^{t_0}(t) C^{\widetilde{s}*}_{t_0,0}}, \\ A_t &= \delta(V_{t+1}(s) - V_{t+1}(i)), \\ B_t &= \delta V_{t+1}(i). \end{aligned}$$

The selected contact rate at step t of $\mathcal{M}_{t_0}$ is given by a_t^{h*}, the optimal point of $u^s(a) + \rho^t(a)$. Thus, we have the first order relations:

$$\begin{aligned} &(u^s)'(a^{s*}_{\text{opt}}) = 0 \\ &(u^s)'(a_t^{s*}) - \beta \vartheta_t A_t e^{-\beta \vartheta_t a_t^{s*}} = 0. \end{aligned} \tag{9.1}$$

Therefore, we have

$$\left| (u^s)'(a^{s*}_{\text{opt}}) - (u^s)'(a_t^{s*}) \right| = \beta \vartheta_t |A_t| e^{-\beta \vartheta_t a_t^{s*}} \leq \beta \vartheta_t |A_t|.$$

Suppose ϑ_t and A_t can be bounded uniformly for all $t \in \{t_0, t_0 + 1, \cdots, t_0 + \tau\}$ and all initial conditions of the projection system at t_0, then we would have

$$\left| (u^s)'(a^{s*}_{\text{opt}}) - (u^s)'(a_t^{s*}) \right| \leq M\beta$$

for some $M \in \mathbb{R}_{>0}$. Given $\epsilon > 0$, because $(u^s)'$ is continuous and defined over a compact set of possible contacts, by Lemma 9.1, using $b = 0$ for $f = (u^s)'$, there is $\delta > 0$ such that if $\left| (u^s)'(a^{s*}_{\text{opt}}) - (u^s)'(a_t^{s*}) \right| < \delta$ then $\left| a^{s*}_{\text{opt}} - a_t^{s*} \right| < \epsilon$. Then it would be enough to take $\beta = \frac{\delta}{M}$. Because this inequality is true for all $t \in \{t_0, t_0 + 1, \cdots, t_0 + \tau\}$ then the process $\mathcal{M}_{t_0}$ would end up selecting contact rate $C^{s*}_{t_0}$ with $\left| a^{s*}_{\text{opt}} - C_t^{s*} \right| < \epsilon$. Furthermore, if the bound can be proven to be independent of t_0 then we would have $\Delta(C^h) < \epsilon$ and our proof for limit **(A)** would be complete.

As for limit **(B)**, we use the Mean Value Theorem to find ξ_t between a_t^{s*} and a^{s*}_{opt} such that

$$(u^s)'(a^{s*}_{\text{opt}}) - (u^s)'(a_t^{s*}) = (u^s)''(\xi_t)(a^{s*}_{\text{opt}} - a_t^{s*}).$$

Combining this with equation (9.1) we get

$$-\beta \vartheta_t A_t e^{-\beta \vartheta_t a_t^{s*}} = (u^s)''(\xi_t)(a^{s*}_{\text{opt}} - a_t^{s*}).$$

In consequence, we have

$$|a^{s*}_{\text{opt}} - a^{s*}_t| \leq \frac{\beta\vartheta_t|A_t|}{|(u^s)''(\xi_t)|} \leq \left|\left|\frac{1}{(u^s)''}\right|\right|_{\infty,I} \beta\vartheta_t|A_t|.$$

Therefore, subject to obtaining the necessary bounds, a similar argument from above allows us to complete the proof for limit **(B)** as well.

Consequently, we show how to uniformly bound both A_t and ϑ_t for this differential equation system. For ϑ_t it is simple to see that $\vartheta_t < 1$ independently of t, t_0 or any other model parameter. For $A_t = \delta(V_{t+1}(s) - V_{t+1}(i))$, we recall that

$$\begin{aligned}\big|V_t(h)\big| &= \left|\max_{a\in\mathcal{S}}\left\{u^h(a) + \delta\sum_{h\in h'} p^t_{hh'}(a)V_{t+1}(h')\right\}\right| \\ &\leq ||u^h||_{\infty,I} + \max_{a\in\mathcal{A}}\left|\delta\sum_{h'\in\mathcal{S}} p^t_{hh'}(a)V_{t+1}(h')\right| \\ &\leq ||u^h||_{\infty,I} + \delta\left(\max_{h'\in\mathcal{S}}\big|V_{t+1}(h')\big|\right)\max_{a\in\mathcal{A}}\sum_{h'\in\mathcal{S}} p^t_{hh'}(a)\end{aligned}$$

Using that $P^t(a)$ is a transition probability matrix, then the sum of each of its rows equals one, giving us that

$$\big|V_t(h)\big| \leq ||u^h||_{\infty,I} + \delta\max_{h'\in\mathcal{S}}\big|V_{t+1}(h')\big|$$

for all $h \in \mathcal{S}$, thus

$$\max_{h'\in\mathcal{S}}\big|V_t(h')\big| \leq \max_{h'\in\mathcal{S}}||u^{h'}||_{\infty,I} + \delta\max_{h'\in\mathcal{S}}\big|V_{t+1}(h')\big|.$$

Applying backwards induction, starting at $t = t_0 + \tau$, we have that

$$\max_{h'\in\mathcal{S}}\big|V_t(h')\big| \leq \max_{h'\in\mathcal{S}}||u^{h'}||_{\infty,I}\left(1 + \delta + \delta^2 + \cdots + \delta^{\tau-t-1}\right) + \delta^{\tau-t}\max_{h'\in\mathcal{S}}\big|V_{t_0+\tau}(h')\big|.$$

Using the fact that the initialization point of the MDP $\mathcal{M}_{t_0}$ is given by $V_{t_0+\tau+1}(h') = 0$ for all $h' \in \mathcal{S}$ is simple to see that $V_{t_0+\tau}(h') = \max_{a\in\mathcal{A}} u^h(a) = ||u^h||_{\infty,I}$, and this gives us that

$$\begin{aligned}\max_{h'\in\mathcal{S}}\big|V_t(h')\big| \leq \max_{h'\in\mathcal{S}}||u^{h'}||_{\infty,I}\left(1 + \delta + \delta^2 + \cdots + \delta^{\tau-t-1} + \delta^{\tau-t}\right) = \\ \max_{h'\in\mathcal{S}}||u^{h'}||_{\infty,I}\left(\frac{1-\delta^{\tau-t+1}}{1-\delta}\right) < \max_{h'\in\mathcal{S}}||u^{h'}||_{\infty,I}\left(\frac{1}{1-\delta}\right).\end{aligned}$$

This bound only depends on the utility functions u^h. Consequently, for any t_0 and any $t \in \{t_0, t_0 + 1, \cdots, t_0 + \tau\}$, we have that

$$|A_t| = \big|\delta(V_{t+1}(s) - V_{t+1}(i))\big| \leq 2\delta\max_{h'\in\mathcal{S}}\big|V_{t+1}(h')\big| \leq 2\delta\max_{h'\in\mathcal{S}}||u^{h'}||_{\infty,I}\left(\frac{1}{1-\delta}\right).$$

□

Remark 9.3. Note that, when using the semi-quadratic utility functions from formula (8.1) we have that

$$(u^h)''(a) = 2\nu(b_h \cdot a - a^2)^{\nu-2}\left[b_h \cdot a - a^2 + 2a(\nu-1)\right],$$

In an interval $I = [a_0, a_{\max}]$ with $a_0 > 0$ we have that

$$\lim_{\nu\to 0} ||(u^h)''||_{\infty,I} = 0,$$

thus, justifying the inverse relationship between $\Delta(C^h)$ and the value of ν.

Remark 9.4. Recall that the curvature of a function $y = u(a)$ at a point a_0 is given by

$$\kappa(a_0) = \frac{|y''(a_0)|}{(1 + (y'(a_0))^2)^{3/2}}.$$

If $y'(a_0) = 0$, being a_0 an optimal of y in some interval, then $\kappa(a_0) = |y''(a_0)|$. Thus, we are able to frame the relation between the curvature of the utility function and the adaptive change, in terms of the second derivative of u^h near the utility optimal.

10. Further Applications: Adaptive network models

10.1. **Introduction.** The use of networks in epidemics has become a very useful tool to model complex scenarios that mimic the connections between agents in the development of a disease ([28]). Networks capture the idea of connections between individuals and provide a powerful mathematical construction to represent these connections. That's why, in light of the recent COVID pandemic, there have been many modelling proposals that aim to take advantage of the network resource to better model the outbreak of a disease through contacts between susceptible and infected individuals. Considerable effort was made by the EpiMec group at the University of Costa Rica into developing a network model based on real government data from the beginnings of the COVID-19 pandemic [34, 35, 36, 37].

Our aim in this section will be to exemplify how the adaptive decision process can be applied to network models in their update of connections between nodes (individuals). We will use the network model described in [35] as a basis. Hence, we start by explaining this network model and it's implementation, then we will modify the model with an adaptive algorithm application and finally we will compare results with the initial model.

10.2. **Basic Network Model.** We briefly explain the network model proposed in [34, 35, 36, 37], for more specific details and results we direct the reader to said references. The network is based on a SIR model with the following state compartments: susceptible (S), exposed (E), diagnosed or observed (O), undiagnosed or not observed (U), hospitalized (H), recovered (R), and dead (D). Each individual is labeled with an ID from 1 to N, and there are arrays `IDtoFamily, IDtoCounty, IDtoAge` that store family, county and age index for each individual, respectively.

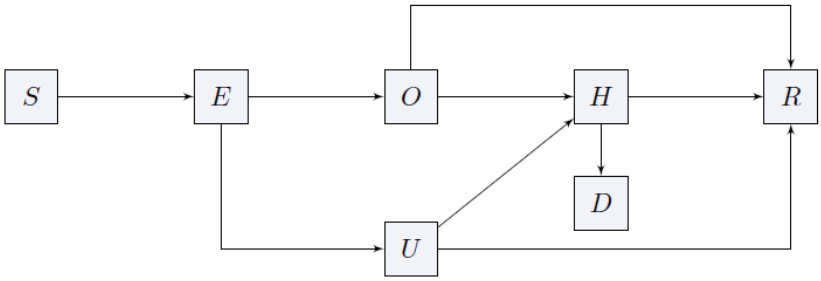

FIGURE 24. Health compartments and transitions for the network model. Figure taken from [37].

This network model is based on a **multi-layer** approach. Each individual engages in contacts with three layers: layer 1 represents the individual's family and close friends, layer 2 represents a middle range coworker circle and layer 3 represents a bigger range coworker circle that can span other counties different than the county that the individual resides in. This model assumes that contacts within an individual's family and very close connections are achieved every day, and that contacts with other circles in the other layers are updated every day.

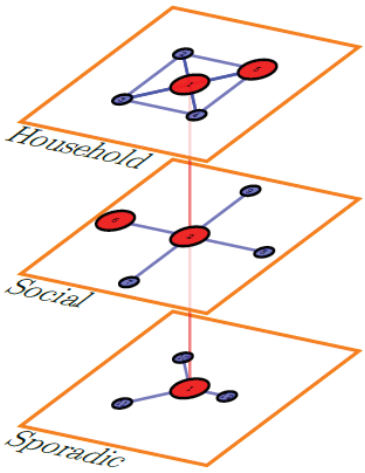

FIGURE 25. The three layers used in the multi-layered network model. Figure taken from [37].

This update on the further layers is currently implemented by considering the contact possibilities within each county and selecting a random number of connections in that range. The model specifies allowed ranges of contact mobility for each county, hence individuals in a county must elect contacts that are bounded by these parameters. The current update occurs, more specifically, like this: *the multi-considers a binary symmetric matrix where its entry (m, n) is equal to 1 if there are connections between counties m and n, and 0 otherwise. This means that the eligible list for a node includes all IDs from counties that have connectivity with its county. We then randomly*

choose the remaining number of contacts for each node from the eligible list. Edges on layer 3 are daily updated in a similar way, excluding preassigned contacts (cited from [35]). This is precisely the step in which we will apply an adaptive approach to select these contact updated, as we will discuss in subsection 10.4.

Once susceptible nodes have elected their daily contacts, it remains to compute the probability that a susceptible node will become infected. This is done by taking into account the node's connections and the health statuses of these connections. The probability is computed as

$$p_i = 1 - \prod_{j \neq i} (1 - \beta_{ij}),$$

where the product goes through all nodes that are connected to node i in a given day, and the values of β_{ij} depend on many factors such as age, health status of the nodes, restriction measures and others. Once p_i is determined, a pseudo-random number $r_i \in (0, 1)$ is computed, and the susceptible node becomes exposed if $p_i < r_i$ (that is, we perform a random experiment to see if the node becomes exposed to the disease).

This part controls the transition from susceptible nodes to being exposed to the disease. For the other transitions, the network model uses transition probabilities which are computed in terms of the number of days an individual has been in a given health status. For example, the transition of exposed to observed o not observed after the node has been exposed for 7 days has a probability of 0.8, so at the eight day of exposure this transition is used to determine if the individual is transferred to the corresponding compartment. Transition probabilities might depend on age groups as well. The pseudo-code for this algorithm is exemplified in [35][Algorithm 1]. It's important to take into account that because updating the entire network can be computationally expensive, the model's implementation only includes the edges between new exposed individuals E and their contacts at each day's iteration. The process keeps a count of how many individuals are in each state every day.

Remark 10.1. To simplify our application to network models we will consider a similar setting, however only including a single category of infected individuals (I). Hence, from now on out networks model will be done with the S, E, I, R health compartments. The network algorithm remains largely the same, with the sole exception of modifying the transition probabilities and the status recordings through time.

Remark 10.2. We note that an application of the adaptive algorithm is certainly not the only path towards adding contact decisions into a network model and several techniques exist to tackle this problem. For example, [31] creates a SAIS model (of susceptible (S), alert (A) and infected (I) individuals) in which there are different contact pools for susceptible and alert individuals and the nodes switch between these contact pools depending on their health status. Another implementation is given by [10] offers a Bayesian model in which the edge connections are computed dynamically depending on layer-specific information and using Gaussian processes to allocate the spatial distribution of contacts through time. On the other hand, [42] creates a model with two

layers which can have interconnections, and the link nodes are randomly rewired through time to avoid contacts between infected and susceptibles in the interconnecting nodes, their results show some epidemic states in which infection can be completely decoupled between the two layers. To our knowledge the method that we will discuss in this section is the first time the adaptive algorithm is applied in deciding node contacts in a multi-layer network model.

10.3. **Optimal contacts economic specification for nodes.** Although the adaptive setting discussed in the previous sections provides a framework to join the individual's economic and epidemiological considerations into their contact engaging decisions, it does so in an aggregated manner. For example if a utility function $u^s(a)$ is specified for susceptible individuals, then this model implies that all susceptible individuals behave with the same utility function. Of course this is completely understandable: in any differential equation's system of this kind, all individuals of a particular health compartment are assumed to behave with the same characteristics.

We cannot deny that the process so far has given us two major advances in a more precise modelling of individual contact decisions. In chapter 1 we saw a way to desegregate contact behaviour by health status, and so far in chapter 2 we have seen how to add a decision process to change contact behaviour through time. We now take a further step in this process and propose a adaptive network model in which this decision is made at the individual level, and not at the general health status level.

By this we mean that, from now on, instead of assigning a general utility functions for individuals of a health compartment, we should specify utility functions for individually. With this approach, we believe that our models will be able to capture a more realistic contact decision process. Naturally, using network models is the ideal tool to model information at the individual level, hence we will employ the network model for this task.

To simplify the application, we will return to the non-relapse case for now, in which only susceptible individuals are faced with an adaptive contact decision task. For each individual in our network we must specify their utility functions a priori. We recall that the decision process is based on a comparison between the individual's personal utility and the current status of the disease, as illustrated in Figure 19, which we recall here.

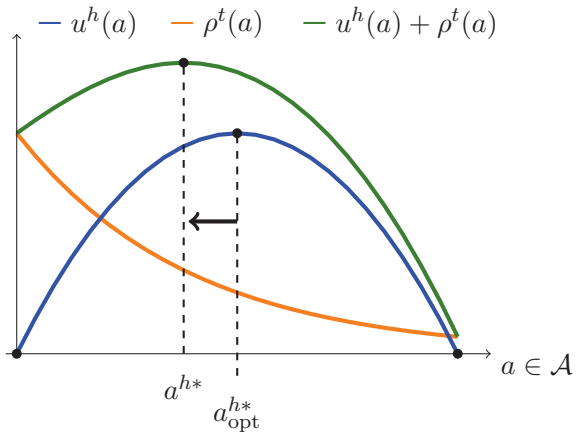

FIGURE 26. Illustration of how the optimality Bellman conditions shift the optimal contact point selected, away from the utility optimal.

Basically, as we see from this figure, when the individual is in health state h, they have an optimal contact decision (the contact that maximizes their personal utility), but the imposition of the disease restriction forces them to consider a reduction in the number of contacts they engage with, causing the final optimum to reduce. As we saw in Figure 21, utility functions with higher curvatures imply a higher rigidity in adapting contact decisions, that is, individuals with a highly curved utility function will be less likely to reduce their contacts away from their optimal contact decision.

Our approach in this section will be to use a Markov Decision Process to compute the selected contacts for susceptible individuals at each step of the network. This process requires to specify utility functions for each health status and transition probability matrices. Each individual will be faced with their own MDP, which will be projected, each day, into a finite horizon into the future.

For each individual we have to create utility functions u^h for each health status. We specify $u^s(a)$ for each agent, an utility function having an optimal a^*_{opt}. Then u^e is created with a smaller optimal point with respect to a^*_{opt}, and likewise with u^i and u^r.

With this information, we start modifying the network implementation from the previous section, by creating two additional arrays: `IDtoOptimal`, which assigns the optimal contact rate (point of utility maximum) to each individual of the population, and `IDtoCurvature` which assigns a label 'high' or 'low' indicating if the individual's utility function will have a higher or lower curvature. This all for the u^s utility function of susceptible state. We now explain how to obtain these vectors from our population settings.

10.3.1. *Creating the `IDtoOptimal` and `IDtoCurvature` vectors.* County level information is important, and the current algorithm implemented in [35] uses a bound on contacts for each county. This variable is called `minmaxBubble` and is an array with a row per county, each containing the minimum and maximum contacts allowed per County, which we will call `min_contacts_county` and `max_contacts_county`. To assign optimal contacts to individuals in a county, we split the county population in three compartments: individuals with high number of optimal contacts, individuals

with a middle number of optimal contacts, and those with a low number of optimal contacts. The split is done by using a predetermined proportion of individuals of each kind, that is, using weights: `prob_high_contact_county, prob_middle_contact_county, prob_low_contact_county` whose sum equals 1. Then for individuals of high contacts, the optimal contact rate is assigned as a random number belonging to the upper 25^{th} quantile of the range of possible contacts per county: [`min_contacts_county`, `max_contacts_county`], for middle sized contacts a random number between the 25^{th} and 75^{th} quantile is assigned, and for low contacts the lower 25^{th} quantile is used to assign optimal contacts.

For the `IDtoCurvature` vector, individuals of high, middle and low contacts in each county are further split into individuals with a high curvature and a low curvature, according to probabilities specified for each subdivision: `p_high_contact_high_curv, p_high_contact_low_curv`, ... `p_low_contact_high_curv, p_low_contact_low_curv`.

10.3.2. *Utility function creation.* For an individual belonging to a given county `C`, who has an optimal decision contact a^*_{opt} and a given curvature specification, we create their utility function as one having the form

$$u^s(a) = (2a^*_{\text{opt}}a - a^2 + c)^\nu,$$

which has a unique global maximum at $a = a^*_{\text{opt}}$. The constant c is computed so that $2a^*_{\text{opt}}a - a^2 + c \geq 0$ for all a in the allowed contact range for county `C`. The parameter ν controls the utility function curvature and it's selected specifying the value of $(u^s)''(a^*_{\text{opt}}) = -2\nu(a^*_{\text{opt}})^{2(\nu-1)}$ for high or low curvatures (the idea is that the curvature is specified in a neighborhood of the optimal point).

Once that the individual's (economical) utility information is specified, we can include the adaptive decision process inside the network's contact daily update. We explain this process in the following section.

10.4. **Contact decision process.** We note that the network model from [36] has no relapse phenomena, hence the only individuals that require a decision process are the susceptibles (as we also pointed out when introducing the adaptive algorithm). The current contact selection algorithm works as follows. At a day step, we obtain the possible coworker contacts for a susceptible individual (layers 2 and 3). If this collection has more individuals that the susceptible agent's county allows, then we cap them appropriately and perform a random pooling to get the effective contacts the individual engages with. In this phase we believe we can add an adaptive computation of the contacts to select.

To do this, we create an MDP process for each susceptible individual at each day, with some modifications. We first recall that our MDP processes are made with a finite horizon τ, so that the individual can make a decision based on a possible behavior of the disease in the short term. From sections 10.3.1 and 10.3.2 we have a utility function u^s for the agent in question. The utilities u^e, u^i and u^r are created from u^s reducing the optimal point a^*_{opt} by multipliers which might depend on the county and edge characteristics.

To create a projection and get the probability transition matrices we use a similar procedure as the one described in [12]. We consider an adaptive decision process only using the susceptible

(S), exposed (E), observed (O), unobserved (U) and recovered (R) health statuses. At each time t_0 we create a projection $(S^{t_0}, E^{t_0}, I^{t_0}, R^{t_0})$ from t_0 to $t_0 + \tau$, of the following differential equations system:

$$\begin{aligned}
\frac{dS}{dt} &= -g(\cdot)\beta\frac{SI}{N} + \mu N - \mu S,\\
\frac{dE}{dt} &= g(\cdot)\beta\frac{SI}{N} - (\kappa+\mu)E,\\
\frac{dO}{dt} &= \kappa E - (\gamma+\mu)I,\\
\frac{dR}{dt} &= \gamma I - \mu R.
\end{aligned} \tag{10.1}$$

Where

$$g(\cdot) = C^s_{t_0} \cdot \frac{C^i_{t_0} I^{t_0}(t)}{C^s_{t_0} S^{t_0}(t) + C^e_{t_0} E^{t_0}(t) + C^i_{t_0} I^{t_0}(t) + C^r_{t_0} R^{t_0}(t)}. \tag{10.2}$$

We use initial conditions given by the current values of the network system at time t_0, and using contacts $(C^s_{t_0}, C^e_{t_0}, C^i_{t_0}, C^r_{t_0})$ given by the average contacts made by individuals of each health class, in the agent's county, the day before t_0[7].

We employ the following transition probability matrix:

$$\begin{pmatrix} p^t_{ss}(a) & p^t_{se}(a) & p^t_{si}(a) & p^t_{sr}(a)\\ p^t_{es}(a) & p^t_{ee}(a) & p^t_{ei}(a) & p^t_{er}(a)\\ p^t_{os}(a) & p^t_{oe}(a) & p^t_{ii}(a) & p^t_{or}(a)\\ p^t_{rs}(a) & p^t_{re}(a) & p^t_{ri}(a) & p^t_{rr}(a) \end{pmatrix} = \begin{pmatrix} 1-p^t_{se}(a) & p^t_{se}(a) & 0 & 0\\ 0 & 1-p^t_{ei}(a) & p^t_{ei}(a) & 0\\ 0 & 0 & 1-p^t_{ir}(a) & p^t_{ir}(a)\\ 0 & 0 & 0 & 1 \end{pmatrix}$$

The entries are defined as

$$p^t_{se}(a) = 1 - \exp\left(-\beta a \frac{C^i_{t_0} I^{t_0}(t)}{C^s_{t_0} S^{t_0}(t) + C^e_{t_0} E^{t_0}(t) + C^o_{t_0} O^{t_0}(t) + C^u_{t_0} U^{t_0}(t) + C^r_{t_0} R^{t_0}(t)}\right), \tag{10.3}$$

$$p^t_{ei}(a) = (1 - e^{-\kappa}) \tag{10.4}$$

$$p^t_{ir}(a) = 1 - e^{-\gamma}, \tag{10.5}$$

Where, $1 - e^{-\kappa}$ is the general probability from moving from E to either I, and $1 - e^{-\gamma}$ is the probability of recovery. For the computation of the optimal policy we have fifth-dimensional value function vectors

$$V_t = \begin{pmatrix} V_t(s)\\ V_t(e)\\ V_t(i)\\ V_t(r) \end{pmatrix}, \quad \text{for each } t = t_0, t_0+1, \cdots, t_0+\tau+1.$$

[7]The decision process, as discussed above, assumes the present behaviour of people will be sustained in the upcoming τ days, and it performs the policy decision based on that information.

Each value function is computed using Bellman's equation. There is one for each health status, and they are given by

$$
\begin{aligned}
V_t(s) &= \max_{a\in\mathcal{A}}\left\{u^s(a)+\delta\left[(1-p^t_{se}(a))V_{t+1}(s)+p^t_{se}(a)V_{t+1}(e)\right]\right\},\\
V_t(e) &= \max_{a\in\mathcal{A}}\left\{u^e(a)+\delta\left[p^t_{ee}(a)V_t(e)+p^t_{ei}V_t(i)\right]\right\},\\
V_t(i) &= \max_{a\in\mathcal{A}}\left\{u^i(a)+\delta\left[(1-p^t_{ir}(a))V_t(i)+p^t_{ir}V_t(r)\right]\right\},\\
V_t(r) &= \max_{a\in\mathcal{A}}\left\{u^r(a)+\delta V_{t+1}(r)\right\}. \qquad (10.6)
\end{aligned}
$$

Here $\mathcal{A}$ is given by the possible contacts allowed by the individual's county bubble. After the value function iteration, the value $a^*_{\text{opt}} \in \mathcal{A}$ that maximizes $V_{t_0}(s)$ will be the selected number of contacts for this individual in the network. Subsequently, the network edges will be updated performing a pooling a^*_{opt} nodes out of the agent's possible contacts, updating the network edge information accordingly and continue with the transition probability computation in the general network model.

Remark 10.3. We hope the reader can easily see how to generalize the adaptive algorithm presented in the last section to more complex models which involve more than the three classical compartments (S,I,R). Note the use of remark in the correct formulation of the incidence rate functions. In this case, adding the extra compartment of exposed individuals required a new specification of probability transitions and value functions.

Remark 10.4. Because of time restrictions, numerical experiments and discussions on results have not been completed for this proposal. The current research team is coordinating efforts to continue with this project and provide results on new research articles to come.

11. Discussion

In this chapter we were able to present the theory of the general adaptive algorithms and analyze some of their analytical properties, as well as provide some interesting applications to other model techniques such as multi-layer networks. The adaptive setting is deeply entrenched in the theory of Markov Decision Processes, a vital mathematical tool in modeling optimal decision making in important areas such as Reinforcement Learning. We enunciated the main components of an MDP in order to immediately explain how this construction can be applied in the epidemiology scenario to introduce a method for contact adaptation in epidemics.

We developed the theory with sufficient generality by employing the MDP approach, which lead us to create an implementation that allowed the introduction of adaptive behavior to non-linear relapse models. With this setting we can see contact adaptation not only in susceptible individuals but also in those that are now temporarily recovered, see example 8.4. This satisfied one of our initial objectives: that of studying adaptive behavior in combination with relapse phenomena.

We also continued with further inspections and comparisons that gave us some interesting theoretical problems and completely new insights into the adaptive algorithm's complexities. For instance, in example 8.4 we compared the adaptive model with two non-adaptive, disaggregated models we called the ex-ante and ex-post models. The ex-ante model consisted of the constant disaggregated model with the initial contact rates of the adaptive model, and the ex-post model consists of the constant disaggregated model using the asymptotic contact rates that the adaptive model arrived at. Naturally, the ex-ante model offers a great difference, as it has been observed in literature that adding adaptive behavior often results in a diminished disease prevalence than the one obtained using classical models.

On the other hand, an interesting result was that the ex-post model seems to behave very similarly to the adaptive model in the later stable stages of the disease. These two models differ in the critical stages of the epidemic, but they come close in the stable time periods, close to the equilibrium.

We conjecture this to be the general case -when convergence is achieved in the adaptive algorithm- however the mathematical complexity of the model didn't allow us to formally justify this result. The implications of this conjecture are important theoretically: this implies that the adaptive algorithm manifests itself more profoundly in the critical stages of the disease, and when the health situation becomes more stable, then there are no sufficient incentives to individuals to consider the disease status in their decisions, so the adaptive procedure banishes. Furthermore, this 'non-adaptive' stage can be approximated also using a constant contacts model developed from the beginning of the disease. The confirmation or rebuttal of this result consists of a open question that we obtain from our simulations.

Nonetheless, our simulations did provide us with other results that we were able to state and prove formally. In examples 8.3 and 8.6 we saw how the model's parameters affect the severity of the adaptive algorithm and the final impact on the contact decisions made. Performing a thorough theoretical insight we explain the workings of the adaptive algorithm. Figures like Figure 19 give us a heuristic on how the algorithm works. *A grosso modo*, this method alters the optimal contact rate that individuals have a priori from their utility function and it corrects it using the current and projected disease information. The end result is that the final optimal contacts are shifted to the left depending on the epidemic state.

We saw that th change from the optimal contacts to the final contact decision -called $\Delta(C^h)$ in the text- is highly affected by some model parameters, such as β the infection rate, or the utility function shape, and in Theorem 9.2 we gave an elementary proof of this result [8]. The utility function curvature is now interpreted as the agent's proclivity to change their contacts in view of the disease information. As we saw in Theorem 9.2 and visualized in Figure 21, a higher curvature means that the agent is less inclined to change their optimal contacts when disease information is presented. This provides a mathematical method to model individual willingness to adapt their behavior in epidemic scenarios.

[8] Although the proof uses purely elementary methods, it becomes complex due to the iterative nature of the algorithm. This is the main challenge that the adaptive setting brings forth to the mathematical analysis.

Unfortunately, the complexity of the adaptive algorithm makes it very difficult to compare bifurcation results such as it was done in Chapter one. In example 8.12 we see that the behavior of the contact rate functions $\kappa(t) := \frac{C_t^{i*}}{C_t^{\tilde{s}*}}$ and $\theta(t) := \frac{C_t^{\tilde{s}*}}{C_t^{s*}}$ is highly dependant of the time, and the adaptive algorithm changes the final ratios, after the critical period of the disease. This implies that the initial conditions are not determinant enough to determine final equilibria. We see this in graphs from Figure 22, which show a more complex behavior than the corresponding graphs from the disaggregated model (Figures 1 and 2).

With the numerical experiments and theoretical results obtained so far we expect to show the power and complexity of the adaptive approach and illustrate the advantages this method offers in modeling contact decisions. We hope that the reader was able to grasp the true workings of the adaptive method and understand it as what it truly is: an intelligent adaptation of the optimal utilitarian contact rates by means of weighting in the epidemiological information.

Finalizing this exploration of the adaptive algorithm we proceeded to study its application in more complex model dynamics. For this we considered the multi-layered network approach. Using the standard formulation of a network model, we incorporated contact utility information at the node level and were able to include a decision process that uses the adaptive algorithm in order to compute the number of contacts for each node.

References

[1] R. Anderson and R. May. Population biology of infectious diseases: Part I. *Nature*, 280:361–367, 1979. ↑4

[2] T. Ash, A. M. Bento, D. Kaffine, A. Rao, and A. I. Bento. Disease-economy trade-offs under alternative epidemic control strategies. *Nat Commun*, 13(3319), 2022. ↑v, ↑vi, ↑1

[3] S. Blythe, K. Cooke, and C. Castillo-Chavez. Autonomous risk-behavior change, and non-linear incidence rate, in models of sexually transmitted diseases. *Biometrics Unit Technical Report*, B-1048-M, 1991. ↑13

[4] F. Brauer. Mathematical epidemiology is not an oxymoron. *BMC Public Health*, 9(Suppl 1):S2, 2009. ↑4

[5] J. Calvo, A. Hernández, M. Porter, and F. Sánchez. A two-patch epidemic model with nonlinear reinfection. *Revista de Matemática Teoría y Aplicaciones*, 27(1):23–48, 2020.

[6] J. Calvo-Monge. Adaptive Behavior for Epidemiological Models. `https://github.com/JimmyCalvoMonge/adaptive`, 2023. ↑31

[7] J. Calvo-Monge, F. Sanchez, J. G. Calvo, and D. Mena. A nonlinear relapse model with disaggregated contact rates: Analysis of a forward-backward bifurcation. *Infectious Disease Modelling*, 8(3):769–782, 2023. ↑2, ↑4

[8] G. Chowell, M. Miller, and C. Viboud. Seasonal influenza in the united states, france, and australia: Transmission and prospects for control. *Epidemiology & Infection*, 136(6):852–864, 2008. ↑16

[9] F. Di Lauro, L. Berthouze, M. D. Dorey, J. C. Miller, and I. Z. Kiss. The impact of contact structure and mixing on control measures and disease-induced herd immunity in epidemic models: A mean-field model perspective. *Bulletin of Mathematical Biology*, 83(117), 2021. ↑4

[10] D. Durante, N. Mukherjee, and R. C. Steorts. Bayesian learning of dynamic multilayer networks. *Journal of Machine Learning Research*, 18(43):1–29, 2017. ↑46

[11] M. Eisermann. The Fundamental Theorem of Algebra Made Effective: An Elementary Real-Algebraic Proof via Sturm Chains. *The American Mathematical Monthly*, 119, 08 2008. ↑21

[12] B. Espinoza, M. Marathe, S. Swarup, and M. Thakur. Asymptomatic individuals can increase the final epidemic size under adaptive human behavior. *Sci Rep*, 11(19744), 2021. ↑v, ↑vi, ↑1, ↑5, ↑49

[13] B. Espinoza, S. Swarup, C. L. Barrett, and M. Marathe. Heterogeneous adaptive behavioral responses may increase epidemic burden. *Sci Rep*, 12(11276), 2022. ↑v, ↑vi, ↑1, ↑5, ↑18

[14] E. P. Fenichel. Economic considerations for social distancing and behavioral based policies during an epidemic. *J. Health Econ.*, 32:440–451, 2013. ↑v, ↑vi, ↑1

[15] E. P. Fenichel, C. Castillo-Chavez, M. G. Ceddia, G. Chowell, P. A. G. Parra, G. J. Hickling, G. Holloway, R. Horan, B. Morin, C. Perrings, M. Springborn, L. Velazquez, and C. Villalobos. Adaptive human behavior in epidemiological models. *Proc. Natl. Acad. Sci. U.S.A.*, 108(15):6306–6311, 2011. ↑v, ↑vi, ↑viii, ↑1, ↑3, ↑5, ↑18, ↑29, ↑31, ↑32, ↑33, ↑37

[16] S. Funk, M. Salathé, and V. Jansen. Modelling the influence of human behaviour on the spread of infectious diseases: a review. *J. R. Soc. Interfac*, 7:1247–1256, 2010. ↑5

[17] N. Goeyvaerts, L. Willem, K. Van Kerckhove, Y. Vandendijck, G. Hanquet, P. Beutels, and N. Hens. Estimating dynamic transmission model parameters for seasonal influenza by fitting to age and season-specific influenza-like illness incidence. *Epidemics*, 13:1–9, 2015. ↑16

[18] A. Gumel. Causes of backward bifurcations in some epidemiological models. *Journal of Mathematical Analysis and Applications*, 395(1):355–365, 2012. ↑2

[19] H. Hethcote. The mathematics of infectious diseases. *SIAM Review*, 42(2), 2000. ↑7

[20] H. Hethcote and P. van den Driessche. Some epidemiological models with nonlinear incidence. *J Math Biol.*, 29(3), 1991. ↑5

[21] Z. Hu, W. Ma, and S. Ruan. Analysis of sir epidemic models with nonlinear incidence rate and treatment. *Mathematical Biosciences*, 238(1):12–20, 2012. ↑5

[22] L. Kallenberg. Markov Decision Processes. `https://www.math.leidenuniv.nl/~kallenberg/Lecture-notes-MDP.pdf`, 2016. [Online; accessed 12-December-2022]. ↑26

[23] G. Li and Y. Zhang. Dynamic behaviors of a modified SIR model in epidemic diseases using nonlinear incidence and recovery rates. *PLoS ONE*, 12(4), 2017. ↑5

[24] W. Liu, H. Hethcote, and S. Levin. Dynamical behavior of epidemiological models with nonlinear incidence rates. *J. Math. Biol.*, 25(4):359–80, 1987. ↑5

[25] S. Moghadas and M. Alexander. Bifurcations of an epidemic model with non-linear incidence and infection-dependent removal rate. *Math Med Biol*, 23(3), 2006. ↑5

[26] B. Morin, E. P. Fenichel, and C. Castillo-Chavez. SIR dynamics with economically driven contact rates. *Nat Resour Model*, 26(4), 2013. ↑v, ↑vi, ↑1, ↑5, ↑13

[27] J. Mossong, N. Hens, M. Jit, P. Beutels, K. Auranen, R. Mikolajczyk, M. Massari, S. Salmaso, G. Tomba, J. Wallinga, J. Heijne, M. Sadkowska-Todys, M. Rosinska, and W. Edmunds. Social contacts and mixing patterns relevant to the spread of infectious diseases. *PLoS Med*, 25(5), 2008. ↑4

[28] M. E. J. Newman. *Networks: an introduction*. Oxford University Press, Oxford; New York, 2010. ↑44

[29] M. Nicola, Z. Alsafi, C. Sohrabi, A. Kerwan, A. Al-Jabir, C. Iosifidis, M. Agha, and R. Agha. The socio-economic implications of the coronavirus pandemic (covid-19): A review. *Int J Surg.*, 78:185–193, 2020. ↑1

[30] A. Rao and T. Jelvis. *Foundations of Reinforcement Learning with Applications in Finance*. Chapman & Hall, London, 2022. ↑26

[31] F. D. Sahneh, A. Vajdi, J. Melander, and C. M. Scoglio. Contact adaption during epidemics: A multilayer network formulation approach. *IEEE Transactions on Network Science and Engineering*, 6(1):16–30, 2019. ↑46

[32] F. Sanchez, J. Arroyo-Esquivel, and J. G. Calvo. A mathematical model with nonlinear relapse: conditions for a forward-backward bifurcation. *Journal of Biological Dynamics*, 17(1):2192238, 2023. PMID: 36942364. ↑2, ↑5, ↑7, ↑8, ↑9, ↑16, ↑21

[33] F. Sanchez, L. A. Barboza, D. Burton, and A. Cintrón-Arias. Comparative analysis of dengue versus chikungunya outbreaks in costa rica. *Ricerche di Matematica*, 67:163–174, 2018. ↑19, ↑20

[34] F. Sanchez, J. G. Calvo, Y. E. García, P. Vásquez, and L. A. Barboza. An implementation of a multilayer network model for the covid-19 pandemic: A costa rica study. *Mathematical Biosciences and Engineering*, 20(1):534–551, 2023. ↑44

[35] F. Sanchez, J. G. Calvo, Y. E. García, P. Vásquez, and L. A. Barboza. A multilayer network model implementation for covid-19. pages 534–551, 2023. ↑3, ↑44, ↑46, ↑48

[36] F. Sanchez, J. G. Calvo, G. Mery, Y. E. García, P. Vásquez, L. A. Barboza, M. D. Pérez, and T. Rivas. A multilayer network model of covid-19: Implications in public health policy in costa rica. *Epidemics*, 39, 2022. ↑44, ↑49

[37] F. Sanchez, J. G. Calvo, G. Mery, Y. E. García, P. Vásquez, L. A. Barboza, M. D. Pérez, and T. Rivas. Projecting the impact of covid-19 variants and vaccination strategies in disease transmission using a multilayer network model in costa rica. *Nature*, 12(2279), 2022. ↑ix, ↑44, ↑45

[38] F. Sanchez, J. G. Calvo, E. Segura, and Z. Feng. A partial differential equation model with age-structure and nonlinear recidivism: Conditions for a backward bifurcation and a general numerical implementation. *Computers & Mathematics with Applications*, 78(12):3916–3930, 2019. ↑6

[39] F. Sanchez, X. Wang, C. Castillo-Chavez, D. Gorman, and P. Gruenewald. Drinking as an epidemic: A simple mathematical model with recovery and relapse. In *Therapist's guide to evidence based relapse prevention*. Burlington: Academic Press, 2007. ↑6, ↑8, ↑16

[40] M. Springborn, G. Chowell, M. MacLachlan, and E. P. Fenichel. Accounting for behavioral responses during a flu epidemic using home television viewing. *BMC Infect Dis.*, 15(21), 2015. ↑v, ↑vi, ↑1, ↑5

[41] H. Tasman, D. Aldila, P. Dumbela, M. Ndii, F. Fatmawati, H. F.F., and C. Chukwu. Assessing the Impact of Relapse, Reinfection and Recrudescence on Malaria Eradication Policy: A Bifurcation and Optimal Control Analysis. *Trop. Med. Infect. Dis.*, 263(7), 2022. ↑20

[42] F. Vazquez, M. A. Serrano, and M. S. Miguel. Rescue of endemic states in interconnected networks with adaptive coupling. *Scientific Reports*, 6(1):2045–2322, 2016. ↑46

[43] D. Xiao and S. Ruan. Global analysis of an epidemic model with non monotone incidence rate. *Math Biosci.*, 208(2):419–429, 2007. ↑5

[44] Y. Xiao and S. Tang. Dynamics of infection with nonlinear incidence in a simple vaccination model. *Nonlinear Anal. Real World Appl.*, 11(5):4154–4163, 2010. ↑5

[45] J. Zhang, M. Litvinova, Y. Liang, Y. Wang, W. Wang, S. Zhao, Q. Wu, S. Merler, C. Viboud, A. Vespignani, M. Ajelli, and H. Yu. Changes in contact patterns shape the dynamics of the COVID-19 outbreak in China. *Science*, 368(6498), 2020. ↑4